

Classical and relativistic long-term time variations of some observables for transiting exoplanets

L. Iorio^{1*}†

¹*Ministero dell’Istruzione, dell’Università e della Ricerca (MIUR), Fellow of the Royal Astronomical Society (FRAS), Italy*

Accepted 2010 September 8. Received 2010 September 8; in original form 2010 July 16

ABSTRACT

We analytically work out the long-term, i.e. averaged over one orbital revolution, time variations $\langle \dot{Y} \rangle$ of some direct observable quantities Y induced by classical and general relativistic dynamical perturbations of the two-body pointlike Newtonian acceleration in the case of transiting exoplanets moving along elliptic orbits. More specifically, the observables Y with which we deal are the transit duration Δt_d , the radial velocity V_ρ , the time interval Δt_{ecl} between primary and secondary eclipses, and the time interval P_{tr} between successive primary transits. The dynamical effects considered are the centrifugal oblateness of both the star and the planet, their tidal bulges mutually raised on each other, a distant third body X , and general relativity (both Schwarzschild and Lense-Thirring). We take into account the effects due to the perturbations of all the Keplerian orbital elements involved in a consistent and uniform way. First, we explicitly compute their instantaneous time variations due to the dynamical effects considered and substitute them in the general expression for the instantaneous change of Y ; then, we take the overall average over one orbital revolution of the so-obtained instantaneous rate $\dot{Y}(t)$ specialized to the perturbations considered. In contrast, previous published works have often employed somewhat “hybrid” expressions, in which the secular precession of, typically, the periastron only is straightforwardly inserted into instantaneous formulas. The transit duration is affected neither by the general relativistic Schwarzschild-type nor by the classical tidal effects, while the bodies’ centrifugal oblatenesses, a distant third body X and the general relativistic Lense-Thirring-type perturbations induce non-vanishing long-term, harmonic effects on Δt_d also for circular orbits. For exact edge-on configurations they vanish. Both V_ρ and Δt_{ecl} experience non-vanishing long-term, harmonic variations, caused by all the perturbations considered, only for non-circular orbits. Also P_{tr} is affected by all of them with long-term signatures, but they do not vanish for circular orbits. Numerical evaluations of the obtained results are given for a typical star-planet scenario and compared with the expected observational accuracies over a time span $\tau = 10$ yr long. Also graphical investigations of the dependence of the effects considered on the semi-major axis and the eccentricity are presented. Our results are, in principle, valid also for other astronomical scenarios. They may allow, e.g., for designing various tests of gravitational theories with natural and artificial bodies in our solar system.

Key words: gravitation-planetary systems-stars: rotation-stars: binaries: eclipsing

1 INTRODUCTION

In several papers somewhat “hybrid” expressions for certain observable quantities pertaining to exoplanets are presented. In them, formulas for the long-term, i.e. averaged over one

orbital revolution, precession of the periastron ω due to some dynamical perturbations are straightforwardly substituted in expressions which, instead, contain instantaneous values of the true anomaly f of the planet. Moreover, a certain lack of uniformity in the various treatments tend to make them, perhaps, difficult to follow.

In this paper we propose a more uniform approach by systematically working out, in an analytic and explicit way whenever possible and/or convenient, the expressions

* E-mail: lorenzo.iorio@libero.it

† Present address: Viale Unità di Italia 68, 70125, Bari (BA), Italy.

for the long-term variations of various observables induced by a number of dynamical perturbations, both of classical and general relativistic origin. In particular, we will focus on the long-term variations of the transit duration Δt_d , the radial velocity V_ρ , the time interval Δt_{ecl} between primary and secondary eclipses, and the time P_{tr} elapsed between consecutive primary transits. Concerning general relativity, the issue of the measurability of certain effects of it in some extrasolar planets has been treated in Miralda-Escudé (2002); Adams & Laughlin (2006a,b,c); Iorio (2006); Heyl & Gladman (2007); Jordán & Bakos (2008); Pál & Kocsis (2008); Ragozzine & Wolf (2009); Li (2010); Iorio (2010). In particular, the perspectives in measuring the correction to the third Kepler law have been considered by Iorio (2006) and Ragozzine & Wolf (2009). Miralda-Escudé (2002), Heyl & Gladman (2007), Jordán & Bakos (2008), Pál & Kocsis (2008) and Ragozzine & Wolf (2009) dealt with the possibility of detecting the gravitoelectric periastron precessions, while Li (2010) looked at the gravitoelectric secular change of the mean anomaly \mathcal{M} connected to the variation of the periastron time transit t_p . Adams & Laughlin (2006a,b,c) studied the impact of the general relativistic gravitoelectric terms on the long-term, secular interactions among multiple planetary systems. Iorio (2010) looked at the relativistic effects induced by the rotation of the hosting star.

In our calculation, we consistently take into account the perturbations of all the Keplerian orbital elements in the following way. Let us assume that an explicit expression is available for a given observable Y in such a way that it is function of all or some Keplerian orbital elements, i.e. $Y = Y(f, \{\kappa\})$, where κ denotes the ensemble of the Keplerian orbital elements explicitly entering Y apart from the mean anomaly \mathcal{M} . Then, we straightforwardly compute its long-term variation as the sum of two parts. The first one is purely Keplerian, and it vanishes over one orbital period P_b . The second one is due to the non-Keplerian variations of all the orbital elements induced by the dynamical perturbation considered. The total result is, thus¹,

$$\begin{aligned} \left\langle \frac{dY}{dt} \right\rangle &= \frac{\Delta Y}{P_b} = \left(\frac{1}{P_b} \right) \int_0^{2\pi} \left[\frac{\partial Y}{\partial f} \frac{df}{d\mathcal{M}} \frac{d\mathcal{M}}{dt} + \right. \\ &+ \left. \sum_{\kappa} \frac{\partial Y}{\partial \kappa} \frac{d\kappa}{dt} \right] \left(\frac{dt}{df} \right) df. \end{aligned} \quad (1)$$

In it, $d\mathcal{M}/dt$ and $d\kappa/dt$ are the instantaneous variations² of the Keplerian orbital elements computed with, e.g., the Gauss variation equations and evaluated onto the unperturbed Keplerian ellipse, while $df/d\mathcal{M}$ and dt/df are the usual Keplerian expressions for such derivatives: see eq. (8) and eq. (9) below. To make easier for the reader to go through the details of the following calculations, we list in Table 1 all the symbols used along with their definitions. More details are also given in the text.

In order to give just some preliminary numerical estimates of the effects computed, we will consider a rather typical star-planet scenario summarized in Table 2. It in-

Table 2. Reference stellar and planetary parameters adopted in the text. We use $M_\star = M_\odot$, $R_\star = R_\odot$, $J_2^\star = J_2^\odot$ (Pireaux et al. 2007), $S_\star = S_\odot$ (Pijpers 1998, 2003), $k_{2\star} = 0.03$ (Claret 1995), $m_p = m_{\text{Jup}}$, $r_p = r_{\text{Jup}}$, $k_{2p} = 0.6$ (Ragozzine & Wolf 2009). Concerning j_2^p , we computed it from $j_2^p = (k_{2p}/3)(n^2 r_p^3 / G m_p)$ (Ragozzine & Wolf 2009), where we assumed that the rotational frequency of the planet is equal to the orbital one n because of tidal effects. For simplicity, we assume that the equators of both the star and the planet coincide with the orbital plane, so that $\Psi_\star = \psi_p = 0$. Moreover, we assume an edge-on orbital configuration, i.e. $i = 90$ deg.

Parameter (units)	Numerical value
M_\star (kg)	1.98895×10^{30}
R_\star (m)	6.9599×10^8
S_\star (kg m ² s ⁻¹)	190.0×10^{39}
J_2^\star	2×10^{-7}
$k_{2\star}$	0.03
m_p (kg)	1.89×10^{27}
r_p (m)	6.991×10^7
k_{2p}	0.6
j_2^p	3×10^{-4}
a (au)	0.04
n (s ⁻¹)	2.5×10^{-5}
P_b (d)	2.9
e	0.07
i (deg)	90
Ψ_\star (deg)	0
ψ_p (deg)	0

cludes a Sun-like host star harboring a close Jupiter-sized planet moving in the equatorial plane of the star along a moderately elliptic orbit. The orbital angular momentum is perpendicular to the line of sight, so that the orbit is in an edge-on configuration. We assume that the rotation of the planet has been locked by tidal effects to the orbital frequency n , and that all the spins of the system are aligned. The meaning of the symbols used in Table 2 has been explained in Table 1. However, it must be noted that, if on the one hand, such a scenario is largely representative of most of the transiting exoplanets discovered so far (Torres et al. 2008), on the other hand some planets showing high inclinations of their orbits to the stellar equatorial planes have been discovered in recent times. They are WASP-33b (Collier Cameron et al. 2010), WASP-2b (Collier Cameron et al. 2007), WASP-5b (Anderson et al. 2008; Gillon et al. 2009), WASP-8b (Queloz et al. 2010), WASP-15b (West et al. 2009), WASP-17b (Anderson et al. 2010) and HAT-P-7b (Narita et al. 2009; Winn et al. 2009). Our general expressions are valid also for such class of objects. Moreover, the Kepler mission is expected to detect numerous planets with a wide distribution of both masses and semi-major axes; to a certain extent, it has already started to do that (Borucki et al. 2010). A quantitative extension of our results to such specific exoplanetary scenarios and to others exhibiting not yet explained features which may be accommodated by the effects investigated here may be the subject of a further, more applicative paper.

Let us note that the validity of the formulas obtained is not limited only to exoplanetary scenarios. Indeed, they may be applied also for, e.g., designing new observational tests of general relativity in our solar system with natural

¹ The analytical calculations have been performed with the aid of the software MATHEMATICA.

² Actually, $d\mathcal{M}/dt$ is the sum of the Keplerian mean motion n and a non-Keplerian term, as we will see later. Its Keplerian part yields from eq. (1) the Keplerian variation of Y .

Table 1. Symbols used in the text along with their definitions.

Symbol	Definition
G	Newtonian constant of gravitation
c	Speed of light in vacuum
M	Mass of the primary in the two-body problem
R_e	Equatorial radius of the primary in the two-body problem
J_2	Adimensional quadrupole mass moment of the primary in the two-body problem
S	Angular momentum of the primary in the two-body problem
M_\star	Mass of the star
R_\star	Radius of the star
S_\star	Angular momentum of the star
J_2^\star	Adimensional quadrupole mass moment of the star
$k_{2\star}$	Love number of the star
m_p	Mass of the planet
r_p	Radius of the planet
k_{2p}	Love number of the planet
J_2^p	Adimensional quadrupole mass moment of the planet
$\mathcal{R}_g \doteq G(M_\star + m_p)/c^2$	Gravitoelectric characteristic length of the system
$\chi_g \doteq 2GS_\star/c^2$	Gravitomagnetic characteristic volume per unit time of the system
U_X	Tidal gravitational potential of a distant third body X
m_X	Mass of the third body X
r_X	Distance of the third body X from the star (assumed constant over one orbital period of the planet p)
$\mathcal{K}_X \doteq Gm_X/r_X^3$	Tidal parameter of the third body
$\hat{\mathbf{l}}_X = \{l_x, l_y, l_z\}$	Unit vector pointing towards the third body (assumed constant over one orbital period of the planet p)
r	Star-planet relative distance
a	Semi-major axis of the orbit
$n \doteq \sqrt{G(M_\star + m_p)/a^3}$	Keplerian mean motion of the orbit
$P_b \doteq 2\pi/n$	Orbital period
e	Eccentricity of the orbit
$p \doteq a(1 - e^2)$	Semilatus rectum of the orbit
v	Speed of the planet along its orbit (assumed elliptical)
i	Inclination of the orbit to the plane of the sky
I_\star	Inclination of the angular momentum of the star to the plane of the sky
Ψ_\star	Inclination of the orbit to the equatorial plane of the star
ψ_p	Inclination of the orbit to the equatorial plane of the planet
f	True anomaly of the orbit
ω	Argument of pericenter of the orbit
Ω	Longitude of the ascending node of the orbit
$u \doteq \omega + f$	Argument of latitude of the orbit
\mathcal{M}	Mean anomaly of the orbit
$\{\kappa\}$	Set of Keplerian orbital elements (apart from the mean anomaly)
$\eta_g \doteq \chi_g n a^{-2} (1 - e^2)^{-7/2} (1 + e \cos f)^3$	Gravitomagnetic characteristic acceleration parameter of the system
$\hat{\mathbf{R}}$	Unit vector along the radial direction of the co-moving frame
$\hat{\mathbf{T}}$	Unit vector along the transverse direction of the co-moving frame
$\hat{\mathbf{N}}$	Unit vector along the normal direction of the co-moving frame
\mathbf{A}	Perturbing acceleration caused by relativity, oblateness, etc.
$A_R \doteq \mathbf{A} \cdot \hat{\mathbf{R}}$	Radial component of the perturbing acceleration
$A_T \doteq \mathbf{A} \cdot \hat{\mathbf{T}}$	Transverse component of the perturbing acceleration
$A_N \doteq \mathbf{A} \cdot \hat{\mathbf{N}}$	Normal component of the perturbing acceleration
$\hat{\mathbf{S}}_\star$	Unit vector along the angular momentum of the star
$\hat{\mathbf{L}}$	Unit vector along the orbital angular momentum
$\hat{\boldsymbol{\rho}}$	Unit vector along the line of sight (pointing towards the observer)
Y	Generic observable quantity
\dot{Y}	Instantaneous time variation of the generic observable quantity Y
ΔY	Net change of the generic observable quantity Y after one orbital revolution
$\langle \dot{Y} \rangle$	Averaged time variation of the generic observable quantity Y
τ	Observational time interval
$\sigma_{\dot{Y}}$	Accuracy in measuring \dot{Y}
$\delta (\bar{\delta})$	Latitude of the transit for elliptic orbits (circular orbits)
Δt_d	Transit duration
V_ρ	Radial velocity
K	Semi-amplitude of the radial velocity curve
V_0	Radial velocity of the center of mass of the system
Δt_{ecl}	Time span between the primary and the secondary eclipses
P_{tr}	Time span between two consecutive primary eclipses

and artificial bodies. In principle, they can be adapted to modified models of gravity as well. The latter aspect will be developed in further studies.

The paper is organized as follows. In Section 2 we illustrate the main features of the classical and relativistic perturbing accelerations considered useful for our purposes. The time variations of the duration transit are worked out in Section 3. Section 4 deals with the time changes of the radial velocity. Section 5 is devoted to the time interval elapsed between primary and secondary eclipses and its long-term temporal variations. The time span between consecutive primary transits is investigated in Section 6. In Section 7 we summarize our results.

2 THE PERTURBING ACCELERATIONS

Here we deal with a generic perturbing acceleration \mathbf{A} induced by some classical and general relativistic dynamical effects.

First, \mathbf{A} has to be projected onto the radial, transverse and normal orthogonal unit vectors $\hat{\mathbf{R}}, \hat{\mathbf{T}}, \hat{\mathbf{N}}$ of the moving frame of the test particle orbiting the central body acting as source of the gravitational field. Their components, in cartesian coordinates, are (Montenbruck & Gill 2000)

$$\hat{\mathbf{R}} = \begin{pmatrix} \cos \Omega \cos u - \cos \Psi \sin \Omega \sin u \\ \sin \Omega \cos u + \cos \Psi \cos \Omega \sin u \\ \sin \Psi \sin u \end{pmatrix} \quad (2)$$

$$\hat{\mathbf{T}} = \begin{pmatrix} -\sin u \cos \Omega - \cos \Psi \sin \Omega \cos u \\ -\sin \Omega \sin u + \cos \Psi \cos \Omega \cos u \\ \sin \Psi \cos u \end{pmatrix} \quad (3)$$

$$\hat{\mathbf{N}} = \begin{pmatrix} \sin \Psi \sin \Omega \\ -\sin \Psi \cos \Omega \\ \cos \Psi \end{pmatrix}. \quad (4)$$

In eq. (2)-eq. (4), Ω, ω, Ψ are the longitude of the ascending node³, the argument of pericenter, reckoned from the line of the nodes⁴, and the inclination of the orbital plane to the reference $\{xy\}$ plane, respectively. Moreover, $u \doteq f + \omega$ is the argument of latitude. Subsequently, the projected components of \mathbf{A} have to be evaluated onto the Keplerian ellipse

$$r = \frac{p}{1 + e \cos f}, \quad p \doteq a(1 - e^2), \quad (5)$$

where p is the semilatus rectum and a, e are the semi-major axis and the eccentricity, respectively. The cartesian coordinates of the Keplerian motion in space are (Montenbruck & Gill 2000)

$$\begin{aligned} x &= r(\cos \Omega \cos u - \cos \Psi \sin \Omega \sin u), \\ y &= r(\sin \Omega \cos u + \cos \Psi \cos \Omega \sin u), \\ z &= r \sin \Psi \sin u. \end{aligned} \quad (6)$$

³ See also eq. (28) below.

⁴ It is the intersection of the orbital plane with the equatorial plane. See eq. (26) and eq. (28) below.

Then, A_R, A_T, A_N are to be substituted into the right-hand-sides of the Gauss equations for the variations of the Keplerian orbital elements. They are (Roy 2005; Soffel 1989)

$$\begin{aligned} \frac{da}{dt} &= \frac{2}{n\sqrt{1-e^2}} [A_R e \sin f + A_T \left(\frac{p}{r}\right)], \\ \frac{de}{dt} &= \frac{\sqrt{1-e^2}}{na} \{A_R \sin f + A_T [\cos f + \frac{1}{e}(1 - \frac{r}{a})]\}, \\ \frac{d\Psi}{dt} &= \frac{1}{na\sqrt{1-e^2}} A_N \left(\frac{r}{a}\right) \cos u, \\ \frac{d\Omega}{dt} &= \frac{1}{na\sqrt{1-e^2} \sin \Psi} A_N \left(\frac{r}{a}\right) \sin u, \\ \frac{d\omega}{dt} &= -\cos \Psi \left(\frac{d\Omega}{dt}\right) + \frac{\sqrt{1-e^2}}{nae} [-A_R \cos f + \\ &+ A_T \left(1 + \frac{r}{p}\right) \sin f], \\ \frac{dM}{dt} &= n - \frac{2}{na} A_R \left(\frac{r}{a}\right) - \frac{(1-e^2)}{nae} [-A_R \cos f + \\ &+ A_T \left(1 + \frac{r}{p}\right) \sin f], \end{aligned} \quad (7)$$

where $n \doteq \sqrt{G(M_* + m_p)/a^3}$ is the Keplerian mean motion related to the orbital period by $n = 2\pi/P_b$.

As explained in the Introduction, the right-hand-sides of eq. (7), computed for the perturbing accelerations of the dynamical effect considered, have to be inserted into the analytic expression of the time variation dY/dt of the observable Y of interest which, then, must be averaged over one orbital revolution according to eq. (1) by means of (Roy 2005)

$$df = \left(\frac{a}{r}\right)^2 \sqrt{1-e^2} dM, \quad (8)$$

and

$$dt = \frac{(1-e^2)^{3/2}}{n(1+e \cos f)^2} df. \quad (9)$$

2.1 The effect of the stellar oblateness

The external gravitational field of a rotating body undergoes departures from spherical symmetry because of the distortion of its shape due to the resulting centrifugal force. An oblate body of equatorial radius R_e and adimensional quadrupole mass moment J_2 affects the orbital motion of a test particle with a non-central perturbing acceleration (Cunningham 1970; Vrbik 2005)

$$\mathbf{A}^{(J_2)} = -\frac{3J_2 R_e^2 GM}{2r^4} \left\{ \left[1 - 5(\hat{\mathbf{r}} \cdot \hat{\mathbf{S}})^2 \right] \hat{\mathbf{r}} + 2(\hat{\mathbf{r}} \cdot \hat{\mathbf{S}}) \hat{\mathbf{S}} \right\}, \quad (10)$$

where $\hat{\mathbf{S}}$ is the unit vector of the body's angular momentum, chosen here as z axis so that the equatorial plane is the reference $\{xy\}$. We will adopt such a choice for the coordinate axes also for the other dynamical perturbations. According to eq. (2)-eq. (4) and eq. (6), the $R - T - N$ components of

eq. (10) are

$$\begin{aligned}
 A_R^{(J_2)} &= -\frac{3n^2 R_e^2 J_2}{8a(1-e^2)^4} (1 + e \cos f)^4 (1 + 3 \cos 2\Psi + \\
 &+ 6 \sin^2 \Psi \cos 2u), \\
 A_T^{(J_2)} &= -\frac{3n^2 R_e^2 J_2}{2a(1-e^2)^4} (1 + e \cos f)^4 \sin^2 \Psi \sin 2u, \\
 A_N^{(J_2)} &= -\frac{3n^2 R_e^2 J_2}{2a(1-e^2)^4} (1 + e \cos f)^4 \sin 2\Psi \sin u.
 \end{aligned} \tag{11}$$

Note that $[n^2 R_e^2 a^{-1}] = \text{L T}^{-2}$. For $\Psi = 0$, i.e. for equatorial orbits, only the radial component is not zero. For polar orbits, i.e. for $\Psi = 90$ deg, the normal component vanishes, contrary to the radial and transverse ones.

2.2 The effect of general relativity

In its slow-motion and weak-field approximation, the Einstein's general theory of relativity predicts that a slowly rotating central body of mass M and proper angular momentum S induces two kinds of small perturbations on the orbital motion of a test particle. The largest one is dubbed gravitoelectric (Mashhoon 2007), and depends only on the mass M of the body which acts as source of the gravitational field. It is responsible of the the well-known anomalous secular precession of the perihelion of Mercury of $43.98 \text{ arcsec cy}^{-1}$ in the field of the Sun. There is also a smaller perturbation, known as gravitomagnetic (Mashhoon 2007), which depends on the angular momentum S of the central body: it causes the Lense-Thirring (Lense & Thirring 1918) precessions of the node and pericenter of a test particle.

2.2.1 The gravitoelectric, Schwarzschild-like perturbation

By defining

$$\mathcal{R}_g \doteq \frac{G(M_* + m_p)}{c^2}, \tag{12}$$

where c is the speed of light in vacuum, the $R-T-N$ components of the general relativistic gravitoelectric perturbing acceleration are (Soffel 1989)

$$\begin{aligned}
 A_R^{(\text{GE})} &= \frac{n^2 \mathcal{R}_g}{(1-e^2)^3} (1 + e \cos f)^2 (3 + 2e \cos f - e^2 + \\
 &+ 4e^2 \sin^2 f), \\
 A_T^{(\text{GE})} &= \frac{n^2 \mathcal{R}_g}{(1-e^2)^3} (1 + e \cos f)^2 4e \sin f (1 + e \cos f), \\
 A_N^{(\text{GE})} &= 0.
 \end{aligned} \tag{13}$$

Note that $[\mathcal{R}_g] = \text{L}$, so that $[n^2 \mathcal{R}_g] = \text{L T}^{-2}$.

2.2.2 The gravitomagnetic, Lense-Thirring-like perturbation

The $R-T-N$ components of the general relativistic gravitomagnetic perturbing acceleration induced by the rotation of the central body with proper angular momentum S are

(Soffel 1989)

$$\begin{aligned}
 A_R^{(\text{GM})} &= \eta_g \cos \Psi (1 + e \cos f), \\
 A_T^{(\text{GM})} &= -\eta_g e \cos \Psi \sin f, \\
 A_N^{(\text{GM})} &= \eta_g \sin \Psi (1 + e \cos f) [2 \sin u + \\
 &+ e \left(\frac{\sin f \cos u}{1 + e \cos f} \right)],
 \end{aligned} \tag{14}$$

with

$$\eta_g \doteq \frac{\chi_g n}{a^2 (1 - e^2)^{7/2}} (1 + e \cos f)^3, \tag{15}$$

and

$$\chi_g \doteq \frac{2GS}{c^2}. \tag{16}$$

Note that $[\chi_g] = \text{L}^3 \text{T}^{-1}$, so that $[\eta_g] = \text{L T}^{-2}$. For equatorial orbits $A_N^{(\text{GM})} = 0$ and $A_R^{(\text{GM})} \neq 0$, $A_T^{(\text{GM})} \neq 0$. Instead, for polar orbits, i.e. for $\Psi = 90$ deg, only the normal component does not vanish.

2.3 The tidal bulges

By neglecting the lag due to dissipation which is negligible for giant planets (Murray & Dermott 2000), the perturbing acceleration due to the tidal bulge raised on the planet by the host star is entirely radial, so that (Cowling 1938)

$$\begin{aligned}
 A_R^{(\text{tid p})} &= -\left(\frac{M_*}{m_p} \right) \frac{3k_{2p} r_p^5 G(M_* + m_p)}{r^7}, \\
 A_T^{(\text{tid p})} &= 0, \\
 A_N^{(\text{tid p})} &= 0.
 \end{aligned} \tag{17}$$

Here k_{2p} is the Love number of the planet⁵. It measures how the mass redistribution induced by the non-uniform stellar potential actually affects the external gravity field of the planet. Its values are in the range $k_{2p} \approx 0.1 - 0.6$ (Ragozzine & Wolf 2009).

A similar expression holds for the effect due to the tidal bulge raised by the planet on the star: the required substitutions are $M_* \rightarrow m_p$, $m_p \rightarrow M_*$, $r_p \rightarrow R_*$, $k_{2p} \rightarrow k_{2*}$. Bodies with most of their mass near their cores, like main-sequence stars, have very low k_{2*} . It is so because the distorted outer envelope has little mass, thus affecting negligibly the outer gravitational field. Indeed, Claret (1995) yields $k_{2*} \approx 0.03$.

2.4 A distant third body X

The perturbing potential induced by a distant, third body X is (Hogg et al. 1991)

$$U_X = \frac{Gm_X}{2r_X^3} \left[r^2 - 3(\mathbf{r} \cdot \hat{\mathbf{l}}_X)^2 \right], \tag{18}$$

⁵ Here k_{2p} is twice the Love number customarily used in binary stars literature (Cowling 1938).

where $\hat{\boldsymbol{l}}_X \doteq \boldsymbol{r}_X/r_X$ is a unit vector pointing towards X. By denoting l_x, l_y, l_z the direction cosines of \boldsymbol{r}_X , i.e. the components of $\hat{\boldsymbol{l}}_X$, we will express U_X as

$$U_X = \frac{Gm_X}{2r_X^3} [r^2 - 3(xl_x + yl_y + zl_z)^2]. \quad (19)$$

After working out the cartesian components of the perturbing acceleration $\boldsymbol{A}_X = -\nabla U_X$ from eq. (19), the explicit expressions of the $R-T-N$ components can be worked out with the aid of eq. (2)-eq. (4) and eq. (6). They are

$$\begin{aligned} A_R^{(X)} &= \frac{3a(1-e^2)\mathcal{K}_X}{(1+e\cos f)} \left[\mathfrak{R}_s(\Psi_*, \Omega, \hat{\boldsymbol{l}}_X) \sin u + \right. \\ &\quad \left. + \mathfrak{R}_c(\Omega, \hat{\boldsymbol{l}}_X) \cos u \right]^2, \\ A_T^{(X)} &= \frac{3a(1-e^2)\mathcal{K}_X}{(1+e\cos f)} \left[\mathfrak{T}_s(\Psi_*, \Omega, \hat{\boldsymbol{l}}_X) \sin 2u + \right. \\ &\quad \left. + \mathfrak{T}_c(\Psi_*, \Omega, \hat{\boldsymbol{l}}_X) \cos 2u \right], \\ A_N^{(X)} &= \frac{3a(1-e^2)\mathcal{K}_X}{(1+e\cos f)} \left[\mathfrak{N}_s(\Psi_*, \Omega, \hat{\boldsymbol{l}}_X) \sin u + \right. \\ &\quad \left. + \mathfrak{N}_c(\Psi_*, \Omega, \hat{\boldsymbol{l}}_X) \cos u \right], \end{aligned} \quad (20)$$

where

$$\mathcal{K}_X \doteq \frac{Gm_X}{r_X^3} \quad (21)$$

is the so-called tidal parameter; $[\mathcal{K}_X] = \text{T}^{-2}$. Note that both $\hat{\boldsymbol{l}}_X$, which is assumed constant over one orbital revolution of the perturbed planet, and Ω here refer to the stellar equatorial plane.

The coefficients of eq. (20) are

$$\begin{aligned} \mathfrak{R}_s &\doteq l_z \sin \Psi_* + \cos \Psi_* (l_y \cos \Omega - l_x \sin \Omega), \\ \mathfrak{R}_c &\doteq l_x \cos \Omega + l_y \sin \Omega, \\ \mathfrak{T}_s &\doteq \frac{[l_z \sin \Psi_* + \cos \Psi_* (l_y \cos \Omega - l_x \sin \Omega)]^2 - (l_x \cos \Omega + l_y \sin \Omega)^2}{2}, \\ \mathfrak{T}_c &\doteq (l_x \cos \Omega + l_y \sin \Omega) [l_z \sin \Psi_* + \cos \Psi_* (l_y \cos \Omega - \\ &\quad - l_x \sin \Omega)], \\ \mathfrak{N}_s &\doteq [l_z \sin \Psi_* + \cos \Psi_* (l_y \cos \Omega - l_x \sin \Omega)] \times \\ &\quad \times [l_z \cos \Psi_* + \sin \Psi_* (l_x \sin \Omega - l_y \cos \Omega)], \\ \mathfrak{N}_c &\doteq (l_x \cos \Omega + l_y \sin \Omega) [l_z \cos \Psi_* + \sin \Psi_* (l_x \sin \Omega - \\ &\quad - l_y \cos \Omega)]. \end{aligned} \quad (22)$$

Note that, according to eq. (22), eq. (20) vanishes neither for $\Psi_* = 0$ nor for $l_z = 0$. If both the planet and the perturber X are coplanar and lie in the equatorial plane of the star, then $A_N^{(X)} = 0$, while $A_R^{(X)} \neq 0, A_T^{(X)} \neq 0, A_R^{(X)} \neq A_T^{(X)}$, as intuitively expected.

Actually, in view of their complexity, the previous formulas do not allow one to obtain manageable analytic expressions of general validity for the averaged time variations of the observable quantities we are interested in. Thus, in the

following, we will release approximate expressions for such kind of perturbation. However, the exact effects of X can be numerically computed in specific arbitrary exoplanetary scenarios following the procedure discussed in Section 1.

3 TIME VARIATIONS OF THE TRANSIT DURATION IN ELLIPTIC ORBITS

For an unperturbed Keplerian elliptic orbit arbitrarily inclined to the line of sight, the transit duration Δt_d can be written as (Tingley & Sackett 2005; Jordán & Bakos 2008)

$$\Delta t_d = \frac{2(R_* + r_p)}{v} \cos \delta. \quad (23)$$

In it, R_* and r_p are the radii of the star and the planet, respectively. The Keplerian speed of the planet v is (Roy 2005)

$$v = \frac{na}{\sqrt{1-e^2}} \sqrt{1+2e\cos f+e^2}. \quad (24)$$

The latitude δ of the transit on the stellar disk is defined from

$$\sin \delta \doteq \frac{r \cos i}{R_* + r_p}, \quad (25)$$

in which r is given by eq. (5). The parameter i is the angle between the unit vector $\hat{\boldsymbol{L}}$ of the orbital angular momentum and the unit vector $\hat{\boldsymbol{\rho}}$ of the line of sight pointing towards the observer. From the spherical law of cosines (Gellert et al. 1989; Zwillinger 1995)

$$\cos B = \sin C \sin A \cos b - \cos C \cos A \quad (26)$$

with the identifications⁶ $A \rightarrow \Psi_*, B \rightarrow \pi - i, C \rightarrow I_*, b \rightarrow \pi - \Omega$, it turns out

$$\cos i = \sin \Psi_* \sin I_* \cos \Omega + \cos \Psi_* \cos I_*, \quad (27)$$

where Ψ_* is the angle between $\hat{\boldsymbol{L}}$ and the unit vector $\hat{\boldsymbol{S}}_*$ of the star's proper angular momentum, I_* is the angle between $\hat{\boldsymbol{S}}_*$ and $\hat{\boldsymbol{\rho}}$, and Ω is the longitude of the ascending node defined from

$$\sin \Psi_* \sin I_* \cos \Omega = (\hat{\boldsymbol{S}}_* \times \hat{\boldsymbol{L}}) \cdot (\hat{\boldsymbol{S}}_* \times \hat{\boldsymbol{\rho}}). \quad (28)$$

Incidentally, it may be noted from eq. (27) that for equatorial orbits, i.e. for $\Psi_* = 0$, we have $i = I_*$. Thus, Δt_d , for an elliptic orbit, is a function of⁷ f, a, e through v and r in $\cos \delta$, and of Ψ_* and Ω through i in $\cos \delta$. As a consequence, when the effect of a given dynamical perturbation on Δt_d is considered, the variations of all such Keplerian orbital elements have to be fully taken into account.

In the following calculations of the time variation of Δt_d due to various dynamical perturbations the expression

$$\left\{ 1 - \left[\frac{a(1-e^2)\cos i}{(R_* + r_p)(1+e\cos f)} \right]^2 \right\}^{-1/2} \quad (29)$$

⁶ In such a way, Ω results to be prograde with respect to the orbital motion, i.e. Ω follows it, coherently with the definition of the longitude of ascending node.

⁷ We neglect possible time changes of the star's spin axes.

appears: to make computation simpler, we will approximate it with

$$\left\{ 1 - \left[\frac{a(1-e^2)\cos i}{(R_\star + r_p)} \right]^2 \right\}^{-1/2}. \quad (30)$$

3.1 The effect of the stellar oblateness

An exact calculation, valid to all orders in e , cannot be performed because of the difficulty of the integrals involved in the evaluation of eq. (1). Thus, in addition to eq. (30), we have to approximate also eq. (24) entering the integrands with negative powers. We will retain the first order terms in their expansions, which is admissible for $e < \sqrt{2} - 1 \approx 0.4$.

Such an approximate calculation shows that the overall averaged time variation of Δt_d induced by the stellar oblateness does not vanish for elliptic orbits. It turns out that the non-vanishing terms are those due to the perturbations in $a, e, \Psi_\star, \Omega, \omega, \mathcal{M}$. This is a clear example of how simply inserting the long-term precessions of the Keplerian orbital elements into instantaneous expressions would yield incorrect results; indeed, the long-term variations of a, e, Ψ_\star caused by the oblateness of the primary are notoriously zero (Roy 2005). By defining

$$\sin \bar{\delta} \doteq \frac{a \cos i}{(R_\star + r_p)}, \quad (31)$$

we finally have

$$\begin{aligned} \left\langle \frac{d\Delta t_d}{dt} \Big|^{(J_2^\star)} \right\rangle &= - \left(\frac{R_\star}{a} \right)^2 \frac{3J_2^\star \sqrt{1-e^2} \sin \bar{\delta} \sin 2\Psi_\star \sin I_\star \sin \Omega}{2\sqrt{1-(1-e^2)^2 \sin^2 \bar{\delta}}} + \\ &+ \mathcal{O}(e^2). \end{aligned} \quad (32)$$

In the limit $e \rightarrow 0$, eq. (32) reduces to

$$\left\langle \frac{d\Delta t_d}{dt} \Big|_0^{(J_2^\star)} \right\rangle = \frac{2 \tan \bar{\delta} \sin \Psi_\star \sin I_\star \sin \Omega}{n} \left\langle \frac{d\Omega}{dt} \Big|^{(J_2^\star)} \right\rangle, \quad (33)$$

obtained in Iorio (2010) for circular orbits. Indeed (Roy 2005),

$$\left\langle \frac{d\Omega}{dt} \Big|_0^{(J_2^\star)} \right\rangle = -\frac{3}{2} n J_2^\star \left(\frac{R_\star}{a} \right)^2 \cos \Psi_\star \quad (34)$$

for $e \rightarrow 0$. For another derivation of eq. (33), which can be applied to all perturbations when $e \rightarrow 0$, see Section 3.4. Note that, for exactly edge-on orbits, both eq. (32) and eq. (33) vanish. The same occurs if the orbit is equatorial, irrespectively of its inclination to the plane of the sky. It is important to note that the long-term effects of eq. (32)-eq. (33) are not secular trends linearly changing in time because of the presence of Ψ_\star and Ω as arguments of trigonometric functions. Indeed, such Keplerian orbital elements do, in general, slowly vary in time because of dynamical effects like a distant third body X, general relativity, and the oblateness itself.

Finally, let us mention that the oblateness J_2^p of the planet also affects Δt_d in the same way. The related formulas can be obtained from the previous one provided that the substitution $R_\star \rightarrow r_p, J_2^\star \rightarrow J_2^p$ is performed.

3.2 The effect of general relativity

3.2.1 The gravitoelectric, Schwarzschild-like perturbation

From eq. (13) it turns out that the general relativistic gravitoelectric term can only affect $d\Delta t_d/dt$ through its perturbations on a, e, \mathcal{M} . The long-term variations for such Keplerian orbital elements are zero (Soffel 1989), apart from the mean anomaly (Iorio 2007).

Instead, after an approximate calculation valid for $e < \sqrt{2} - 1 \approx 0.4$ analogous to the previous one, it turns out that

$$\left\langle \frac{d\Delta t_d}{dt} \Big|^{(\text{GE})} \right\rangle = 0. \quad (35)$$

The same holds also for circular orbits, as can be immediately seen by inspecting the general method of Section 3.4 which involves the long-term variations of Ψ_\star and Ω .

3.2.2 The gravitomagnetic, Lense-Thirring-like perturbation

According to an approximate calculation in e , valid for $e < \sqrt{2} - 1 \approx 0.4$, analogous to the previous ones, the averaged time variation of Δt_d induced by the general relativistic gravitomagnetic effect is, in general, non-zero for elliptic orbits. In particular, the non-vanishing terms are those due to the perturbations in Ψ_\star and Ω . This is another example of how the mere insertion of the long-term precessions of the Keplerian orbital elements into instantaneous expressions would yield incorrect results; indeed, the Lense-Thirring long-term precession of Ψ_\star vanishes (Lense & Thirring 1918; Soffel 1989).

We have

$$\begin{aligned} \left\langle \frac{d\Delta t_d}{dt} \Big|^{(\text{GM})} \right\rangle &= \left(\frac{GS_\star}{c^2 a^3 n} \right) \frac{\sin \bar{\delta} \sin \Psi_\star}{2\sqrt{1-(1-e^2)^2 \sin^2 \bar{\delta}}} \times \\ &\times [\mathfrak{L}(e, \Omega, \omega, I_\star, \Psi_\star) + \mathfrak{M}(e, \Omega, \omega, I_\star)], \end{aligned} \quad (36)$$

with

$$\begin{aligned} \mathfrak{L} &\doteq e^2 (1 - e^4) (\cos I_\star \sin \Psi_\star - \\ &- \cos \Psi_\star \sin I_\star \cos \Omega) \sin 2\omega, \\ \mathfrak{M} &\doteq (1 - e^2) \left\{ 8 \left[1 - e^2 \left(1 - \frac{e^2}{2} \right) \right] - \right. \\ &- \left. e^2 (1 + e^2) \cos 2\omega \right\} \sin I_\star \sin \Omega; \end{aligned} \quad (37)$$

the term containing \mathfrak{L} comes from the perturbation in Ψ_\star , while the term with \mathfrak{M} is due to $d\Omega/dt$.

For $e \rightarrow 0$, eq. (36)-eq. (37) yield (Iorio 2010)

$$\begin{aligned} \left\langle \frac{d\Delta t_d}{dt} \Big|_0^{(\text{GM})} \right\rangle &= \frac{2 \tan \bar{\delta} \sin \Psi_\star \sin I_\star \sin \Omega}{n} \left(\frac{2GS_\star}{c^2 a^3} \right) = \\ &= \frac{2 \tan \bar{\delta} \sin \Psi_\star \sin I_\star \sin \Omega}{n} \left\langle \frac{d\Omega}{dt} \Big|^{(\text{GM})} \right\rangle. \end{aligned} \quad (38)$$

According to eq. (36)-eq. (38), also the long-term gravitomagnetic time variation of Δt_d is a harmonic one. For exactly edge-on orbits, both eq. (36) and eq. (38) vanish. The same occurs if the orbit is equatorial, independent of its orientation with respect to the line of sight.

3.3 The tidal bulges

It is found that the long-term variations of the duration transit caused by the tidal bulges mutually raised by the planet and the star on each other vanish.

3.4 A distant third body X

It turns out that a distant body X induces a long-term harmonic variation of the duration transit which does not vanish in the limit $e \rightarrow 0$. In this case, we have

$$\left\langle \frac{d\Delta t_d}{dt} \Big|_0^{(X)} \right\rangle = \left(\frac{\mathcal{K}_X}{n^2} \right) 3 \tan \bar{\delta} \bar{\mathfrak{X}}(\hat{l}_X, \Psi_*, I_*, \Omega), \quad (39)$$

with

$$\begin{aligned} \bar{\mathfrak{X}} &\doteq [l_z \cos \Psi_* + \sin \Psi_* (-l_y \cos \Omega + l_x \sin \Omega)] \times \\ &\times \{-l_x \cos \Psi_* \sin I_* + \sin \Psi_* [l_z \sin I_* \sin \Omega + \\ &+ \cos I_* (l_x \cos \Omega + l_y \sin \Omega)]\}. \end{aligned} \quad (40)$$

Note that if both the perturber body X and the perturbed planet lie in the equatorial plane of the host star, i.e. if $\Psi_* = 0$ and $l_z = 0$, then

$$\left\langle \frac{d\Delta t_d}{dt} \Big|_0^{(X)} \right\rangle = 0, \quad (41)$$

independently of the inclination of the orbital plane to the plane of the sky. Instead, if $\Psi_* = 0$, but X is not coplanar with the perturbed planet, the induced long-term variation of the duration transit does not vanish. The duration transit is not affected by X if the orbit of the perturbed planet is exactly edge-on.

It is interesting to note that eq. (39), with eq. (40), can be also obtained in another, simpler way; the following approach is valid for all the dynamical perturbations previously examined. Indeed, for circular orbits the expression for Δt_d of eq. (23) gets simplified in such a way that

$$\frac{d\Delta t_d}{dt} \Big|_0 = \frac{2 \tan \bar{\delta} \sin i}{n} \left(\frac{di}{dt} \right) + \frac{\partial \Delta t_d}{\partial a} \left(\frac{da}{dt} \right). \quad (42)$$

From eq. (27) it turns out

$$\begin{aligned} \sin i \left(\frac{di}{dt} \right) &= (\sin \Psi_* \cos I_* - \cos \Psi_* \sin I_* \cos \Omega) \frac{d\Psi_*}{dt} + \\ &+ \sin \Psi_* \sin I_* \sin \Omega \left(\frac{d\Omega}{dt} \right). \end{aligned} \quad (43)$$

Thus, only for circular orbits it is admissible to straightforwardly use the long-term variations of a , Ψ_* and Ω , as shown by eq. (42)-eq. (43). In the case of the perturbation due to

a distant body X, it turns out from eq. (7)

$$\begin{aligned} \left\langle \frac{da}{dt} \Big|^{(X)} \right\rangle &= 0, \\ \left\langle \frac{d\Psi_*}{dt} \Big|^{(X)} \right\rangle &= \frac{3\mathcal{K}_X(1-e^2)^3}{2n} (l_x \cos \Omega + l_y \sin \Omega) \times \\ &\times [l_z \cos \Psi_* + \sin \Psi_* (l_x \sin \Omega - l_y \cos \Omega)], \\ \left\langle \frac{d\Omega}{dt} \Big|^{(X)} \right\rangle &= \frac{3\mathcal{K}_X \csc \Psi_* (1-e^2)^3}{2n} [l_z \sin \Psi_* + \cos \Psi_* \times \\ &\times (l_y \cos \Omega - l_x \sin \Omega)] [l_z \cos \Psi_* + \\ &+ \sin \Psi_* (l_x \sin \Omega - l_y \cos \Omega)], \end{aligned} \quad (44)$$

contrary to the stellar oblateness and the general relativistic gravitomagnetism for which the long-term precessions of Ψ_* vanish. It turns out that eq. (44), substituted in eq. (42)-eq. (43), yields the same result of eq. (39)-eq. (40).

3.5 Numerical evaluations

A feature common to all the variations of Δt_d previously examined is that they all vanish for exactly edge-on orbits. Moreover, independently of the inclination of the orbital plane to the line of sight, they vanish also for equatorial orbits, apart from the case of X unless it is coplanar with the perturbed planet moving in the star's equatorial plane.

Thus, we assume in the following $i = 87$ deg and $\Psi_* = 15$ deg. With such assumptions we have

$$\begin{aligned} \left| \left\langle \frac{d\Delta t_d}{dt} \Big|^{(J_2^P)} \right\rangle \right| &\lesssim 1 \times 10^{-8}, \\ \left| \left\langle \frac{d\Delta t_d}{dt} \Big|^{(J_2^*)} \right\rangle \right| &\lesssim 9 \times 10^{-10}, \\ \left| \left\langle \frac{d\Delta t_d}{dt} \Big|^{(GM)} \right\rangle \right| &\lesssim 1 \times 10^{-12}, \\ \left| \left\langle \frac{d\Delta t_d}{dt} \Big|^{(\text{tid } *)} \right\rangle \right| &= 0 \\ \left| \left\langle \frac{d\Delta t_d}{dt} \Big|^{(\text{tid } P)} \right\rangle \right| &= 0, \\ \left| \left\langle \frac{d\Delta t_d}{dt} \Big|^{(GE)} \right\rangle \right| &= 0. \end{aligned} \quad (45)$$

By assuming $e = 0$, a third body X with the mass of Jupiter and located at $r_X = 0.1 - 1$ au yields

$$\left| \left\langle \frac{d\Delta t_d}{dt} \Big|^{(Jup)} \right\rangle \right| \lesssim 8 \times 10^{-5} - 8 \times 10^{-8}, \quad (46)$$

according to 39. The effect of an Earth-like perturber $r_X = 0.1 - 1$ au is, instead,

$$\left| \left\langle \frac{d\Delta t_d}{dt} \Big|^{(Ear)} \right\rangle \right| \lesssim 2 \times 10^{-7} - 2 \times 10^{-10}. \quad (47)$$

The time variations of the duration transit induced by the planetary and stellar oblateness for closer orbits, i.e. for

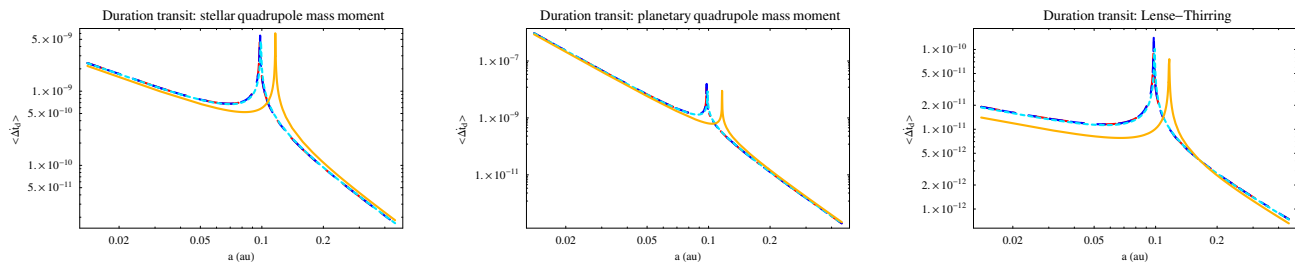


Figure 1. Maximum values of the long-term time variations $\langle \dot{\Delta}t_d \rangle$ as a function of a ($0.014 \text{ au} \leq a \leq 0.449 \text{ au}$) for different values of the eccentricity: $e = 0.005$ (red dash-dotted line), $e = 0.03$ (blue dashed line), $e = 0.1$ (light blue dotted line), $e = 0.4$ (yellow continuous line). For the stellar and planetary physical parameters we used the standard values of Table 2. We adopted $i = 87$ deg, $\Psi_\star = 15$ deg, while we fixed the periastron at $\omega = 90$ deg; we also considered $\sin I_\star \sin \Omega \approx 1$.

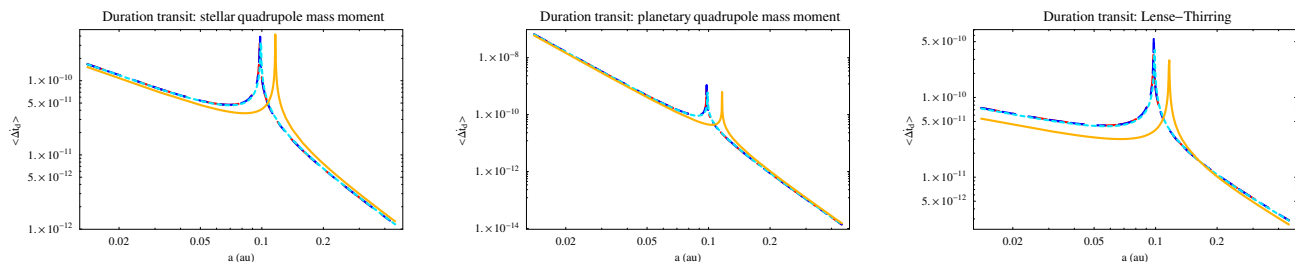


Figure 2. Maximum values of the long-term time variations $\langle \dot{\Delta}t_d \rangle$ as a function of a ($0.014 \text{ au} \leq a \leq 0.449 \text{ au}$) for different values of the eccentricity: $e = 0.005$ (red dash-dotted line), $e = 0.03$ (blue dashed line), $e = 0.1$ (light blue dotted line), $e = 0.4$ (yellow continuous line). For the stellar and planetary physical parameters we used the standard values of Table 2. We adopted $i = 87$ deg, $\Psi_\star = 89$ deg, while we fixed the periastron at $\omega = 90$ deg; we also considered $\sin I_\star \sin \Omega \approx 1$.

$a = 0.015 \text{ au}$, would be of the order of 7×10^{-7} (j_2^p) and 2×10^{-9} (J_2^\star), respectively. In Figure 1 we plot the upper bounds in $\langle \dot{\Delta}t_d \rangle$ due to all the dynamical effects considered, apart from the third body X, as a function of a for different values of the eccentricity. We let a vary within the range of the so-far discovered transiting exoplanets⁸, with a maximum value of e yielding periastron distances not smaller than the star’s radius. We adopted nearly edge-on ($i = 87$ deg) and almost equatorial ($\Psi_\star = 15$ deg) orbital configurations. The physical parameters of the star and the planet have been retrieved from Table 2. It is interesting to look also at almost polar orbital configurations ($\Psi_\star \approx 90$ deg). This is done in Figure 2 obtained for the same values of Figure 1, apart from the inclination of the orbital plane to the stellar equator set now to $\Psi_\star = 89$ deg.

3.6 The observability of the time variation of the transit duration

The accuracy obtainable in measuring the transit duration is of the order of $1.5 - 5$ s; see the accurate discussion in Ford et al. (2008) and Jordán & Bakos (2008). Thus, over an observational time span of $\tau = 10$ yr it should be possible to achieve an accuracy in measuring the time variation of the transit duration of the order of

$$\sigma_{\dot{\Delta}t_d} \approx 5 \times 10^{-9} - 1.6 \times 10^{-8}. \quad (48)$$

A similar conclusion is reached by Miralda-Escudé (2002). Thus, it would be very difficult to measure the effects previously examined with the time variations of the duration transit in typical exoplanetary scenarios, with the possible exception of a third body X.

4 THE RADIAL VELOCITY

The basic observable in spectroscopic studies of exoplanets, transiting or not, is the radial velocity V_ρ . Its expression for elliptic orbits, up to the velocity of the system’s center of mass V_0 , is (Batten 2001)

$$V_\rho = K [e \cos \omega + \cos(f + \omega)], \quad (49)$$

where $2K$ is the total observed range of radial velocity defined by

$$K \doteq \frac{na \sin i}{\sqrt{1 - e^2}}. \quad (50)$$

Perturbing dynamical effects affect the radial velocity as well by inducing, in principle, a non-vanishing net radial acceleration over one orbital period. It can straightforwardly be worked out from eq. (1) with $Y \rightarrow V_\rho$ by noting that, in this case, the perturbations of all the six Keplerian orbital elements are involved.

4.1 The effect of the stellar oblateness

The stellar oblateness causes a long-term harmonic variation of the radial velocity only if the orbit is elliptic. Indeed, it

⁸ See on the WEB <http://www.exoplanet.eu>.

turns out

$$\begin{aligned} \langle \dot{V}_\rho^{(J_2^*)} \rangle &= - \left(\frac{n^2 R_*^2}{a} \right) \frac{3eJ_2^*}{32(1-e^2)^{7/2} \sin i} \times \\ &\times [\mathcal{J}_c(e, i, I_*, \Omega, \Psi_*) \cos \omega + \\ &+ \mathcal{J}_s(e, i, I_*, \omega, \Omega, \Psi_*) \sin \omega], \end{aligned} \quad (51)$$

with

$$\begin{aligned} \mathcal{J}_c &\doteq 10(1-e^2) \cos i \sin I_* \sin 2\Psi_* \sin \Omega, \\ \mathcal{J}_s &\doteq 2(1-e^2) \cos i \sin 2\Psi_* (\cos I_* \sin \Psi_* - \\ &- \sin I_* \cos \Psi_* \cos \Omega) + \sin^2 i [7 + 47 \cos 2\Psi_* + \\ &+ \sin^2 \Psi_* \cos 2\omega - \frac{e^2}{16} (259 + 429 \cos 2\Psi_* - \\ &- 44 \sin^2 \Psi_* \cos 2\omega)]. \end{aligned} \quad (52)$$

It is an exact result in e , and vanishes in the limit $e \rightarrow 0$. Note that, according to eq. (52), eq. (51) vanishes neither for equatorial orbits nor for edge-on configurations.

4.2 The effect of general relativity

Also general relativity affects the radial velocity of non-circular orbits. Indeed, an exact calculation in e yields the following long-term harmonic signatures.

$$\langle \dot{V}_\rho^{(\text{GE})} \rangle = (n^2 \mathcal{R}_g) \frac{15e(1+e^2) \sin i \sin \omega}{8(1-e^2)^{5/2}}, \quad (53)$$

and

$$\begin{aligned} \langle \dot{V}_\rho^{(\text{GM})} \rangle &= \left(\frac{nGS_*}{c^2 a^2} \right) \frac{e}{4(1-e^2)^2} [\mathcal{V}_c(i, I_*, \Omega, \Psi_*) \cos \omega + \\ &+ \mathcal{V}_s(i, I_*, \Omega, \Psi_*) \sin \omega], \end{aligned} \quad (54)$$

with

$$\begin{aligned} \mathcal{V}_c &\doteq 11 \cot i \sin I_* \sin \Psi_* \sin \Omega, \\ \mathcal{V}_s &\doteq \frac{\csc i}{4} \{ \cos \Omega \sin 2I_* (\sin \Psi_* - \sin 3\Psi_*) - \\ &- \sin^2 \Psi_* \cos \Psi_* [\cos 2I_* (3 + \cos 2\Omega) + 2 \sin^2 \Omega] + \\ &+ 104 \sin^2 i \cos \Psi_* \}. \end{aligned} \quad (55)$$

For $e \rightarrow 0$ both eq. (53) and eq. (54) vanish. Also the general relativistic effects are non-vanishing either for edge-on or equatorial orbits, with eq. (53) which is independent of Ψ_* , contrary to eq. (54).

4.3 The tidal bulges

The tidal bulge of the planet induces a non-zero long-term harmonic variation of the radial velocity. Its exact expression

is

$$\begin{aligned} \langle \dot{V}_\rho^{(\text{tid p})} \rangle &= \\ &= \left(\frac{n^2 r_p^5}{a^4} \right) \left(\frac{M_*}{m_p} \right) \times \\ &\times \frac{3e[-496+5e^2(-80+81e^2+8e^4)]k_{2p} \sin i \sin \omega}{128(1-e^2)^{13/2}}. \end{aligned} \quad (56)$$

The long-term variation of the radial velocity due to the tidal bulge raised by the planet on the star is

$$\begin{aligned} \langle \dot{V}_\rho^{(\text{tid } *)} \rangle &= \\ &= \left(\frac{n^2 R_*^5}{a^4} \right) \left(\frac{m_p}{M_*} \right) \times \\ &\times \frac{3e[-496+5e^2(-80+81e^2+8e^4)]k_{2*} \sin i \sin \omega}{128(1-e^2)^{13/2}}. \end{aligned} \quad (57)$$

They vanish for $e \rightarrow 0$ and are independent of Ψ_* .

It is easy to understand that, concerning the tidal distortions, those experienced by the planet are more effective than those suffered by its hosting star. Indeed, eq. (56)-eq. (57) tell us that their ratio goes as

$$\left(\frac{M_*}{m_p} \right)^2 \left(\frac{r_p}{R_*} \right)^5 \frac{k_{2p}}{k_{2*}}. \quad (58)$$

According to Table 2, the ratio of the star-planet masses is typically of the order of 10^3 , while the planet-to-star ratios for the radii and the Love numbers are about 0.1 and 20, respectively.

4.4 A distant third body X

A net non-zero long-term harmonic effect on V_ρ is induced by a distant third body X. Its general expression for arbitrary values of the eccentricity and of the position of X is too cumbersome to be explicitly displayed here; it turns out

$$\langle \dot{V}_\rho^{(X)} \rangle \propto - (a\mathcal{K}_X) \frac{3e(1-e^2)^{3/2}}{8 \sin i} \mathfrak{W}(\Omega, \omega, \Psi_*, \hat{l}_X). \quad (59)$$

The quite complicated function \mathfrak{W} does not vanish for $l_z = 0, \Psi_* = 0$, i.e. if both the perturbed and the perturbing planets lie in the star's equatorial plane. As for the stellar oblateness and general relativity, $\langle \dot{V}_\rho^{(X)} \rangle$ vanishes for $e \rightarrow 0$. It should not be considered as contradictory because it is the otherwise constant velocity V_0 of the system's center of mass that is altered by the perturber X, independently of the relative motion of the perturbed planet and the star.

4.5 Numerical evaluations

The “standard” orbital scenario of Table 2 yields

$$\begin{aligned}
 \left| \left\langle \dot{V}_\rho^{(\text{tid p})} \right\rangle \right| &\leq 4 \times 10^{-7} \text{ m s}^{-2}, \\
 \left| \left\langle \dot{V}_\rho^{(\text{GE})} \right\rangle \right| &\leq 1 \times 10^{-7} \text{ m s}^{-2}, \\
 \left| \left\langle \dot{V}_\rho^{(J_2^B)} \right\rangle \right| &\leq 6 \times 10^{-8} \text{ m s}^{-2}, \\
 \left| \left\langle \dot{V}_\rho^{(J_2^*)} \right\rangle \right| &\leq 3 \times 10^{-9} \text{ m s}^{-2}, \\
 \left| \left\langle \dot{V}_\rho^{(\text{tid } *)} \right\rangle \right| &\leq 2 \times 10^{-9} \text{ m s}^{-2}, \\
 \left| \left\langle \dot{V}_\rho^{(\text{GM})} \right\rangle \right| &\leq 9 \times 10^{-11} \text{ m s}^{-2}.
 \end{aligned} \tag{60}$$

Concerning a distant third body X, for $m_X = m_{\text{Jup}}$, $r_X = 0.1 - 1$ au and $l_z = 0$, i.e by assuming coplanarity with the perturbed planet, we have

$$\left| \left\langle \dot{V}_\rho^{(\text{Jup})} \right\rangle \right| \lesssim 1 \times 10^{-5} - 1 \times 10^{-8} \text{ m s}^{-2}. \tag{61}$$

For an Earth-sized perturber at 0.1 – 1 au we have

$$\left| \left\langle \dot{V}_\rho^{(\text{Ear})} \right\rangle \right| \lesssim 5 \times 10^{-8} - 5 \times 10^{-11}. \tag{62}$$

In Figure 3 we plot the magnitude of the upper bound of $\left\langle \dot{V}_\rho \right\rangle$ for all the dynamical effects considered, apart from a third body X, as a function of the semi-major axis for different values of the eccentricity. Also in this case, we let a vary within the range of the so-far discovered transiting exoplanets⁹, with a maximum value of e yielding periastron distances not smaller than the star’s radius. Table 2 has been used for the values of the physical parameters of the star and the planet, and for the various orbital inclinations i , Ψ_* , ψ_p ; the periastron has been set equal to $\omega = 90$ deg.

4.6 Measurability of the long-term radial acceleration

The present-day level of accuracy in measuring the radial velocity is about 2 m s^{-1} , so that over $\tau = 10$ yr a net radial acceleration should be detectable at a $\approx 3 \times 10^{-9} \text{ m s}^{-2}$ level. Such a guess is confirmed by the case of¹⁰ HD 126614A, monitored for the past 10 yr, for which a secular change of the radial velocity (Howard et al. 2010)

$$\left\langle \dot{V}_\rho^{(\text{meas})} \right\rangle = (5.13 \pm 0.06) \times 10^{-7} \text{ m s}^{-2} \tag{63}$$

⁹ See on the WEB <http://www.exoplanet.eu>.

¹⁰ In addition to the planet HD 126614Ab ($a = 2.35$ au, $e = 0.41$, $P_b = 3.41$ yr), the star HD 126614A has also a faint M dwarf companion of $M_{\text{dw}} \approx 0.3M_\odot$ at a (sky-projected) distance of 33 au. Named HD 126614B, it was discovered with direct observations using adaptive optics and the PHARO camera at Palomar Observatory (Howard et al. 2010). An even more distant M dwarf, dubbed NLTT37349 and with $M_{\text{dw}} \approx 0.2M_\odot$, is also present in the system at a (sky-projected) distance of about 3×10^3 au (Gould & Chanamé 2004).

has been measured. Incidentally, let us note that for HD 126614A none of the “internal” star-planet dynamical effects considered so far (tidal bulges, oblateness, general relativity) can explain¹¹ eq. (63); indeed, the largest one, caused by the general relativistic gravitoelectric field, amounts to just $10^{-12} \text{ m s}^{-2}$. Concerning a distant third body X, it turns out that a Jupiter-sized planet at 2.2 au ($P_b = 3.0$ yr), assumed coplanar with HD 126614Ab in the equatorial plane of their hosting star, would cause a radial acceleration of the order of $5 \times 10^{-7} \text{ m s}^{-2}$. Alternatively, a rocky Earth-like body at 0.32 au ($P_b = 0.17$ yr) or a Neptune-type planet ($m_X = 14m_\oplus$) at 0.75 au ($P_b = 0.6$ yr) would induce the same effect. It must be recalled that the quality of the fit of the 10 yr-long data record by Howard et al. (2010) was not improved, at a statistically significant level, by a two-planet model for a variety of masses and distances for the second one. A brown dwarf-like object ($m_X = 80m_{\text{Jup}} = 7.6 \times 10^{-2}M_\odot$) at 9 au ($P_b = 24.4$ yr) would also be a viable candidate. According to eq. (59), neither NLTT37349 nor HD 126614B can accommodate eq. (63). Indeed, the effect due to the closest M dwarf would be as large as $\lesssim 10^{-8} \text{ m s}^{-2}$, while that due to the farthest one is as small as $10^{-14} \text{ m s}^{-2}$.

5 THE TIME VARIATION OF THE TEMPORAL INTERVAL BETWEEN PRIMARY AND SECONDARY TRANSIT

Another directly observable quantity in transiting exoplanets is the time elapsed Δt_{ecl} between the primary and the secondary eclipses. The primary eclipse occurs when the exoplanet starts to obscure the host star, while the beginning of the secondary eclipse is when the planet starts to be occulted by the star. For circular orbits, Δt_{ecl} is simply half the orbital period, while for eccentric orbits we have a more complicated expression involving e and ω as well. It is (Sterne 1940; Jordán & Bakos 2008)

$$\begin{aligned}
 \Delta t_{\text{ecl}} \doteq (t_{2\text{ecl}} - t_{1\text{ecl}}) - \frac{P_b}{2} &= \frac{P_b}{\pi} \left[\frac{\sqrt{1-e^2} e \cos \omega}{1-(e \sin \omega)^2} + \right. \\
 &\quad \left. + \arctan \left(\frac{e \cos \omega}{\sqrt{1-e^2}} \right) \right], \tag{64}
 \end{aligned}$$

up to terms proportional to $\cot^2 i$.

5.1 Secular time variations of Δt_{ecl}

Non-Keplerian orbital perturbations affect, in principle, Δt_{ecl} by making it vary orbit after orbit with a characteristic long-term pattern. It is possible to analytically work out exact expressions for all the dynamical effects considered, apart from the case of the distant third body X for which an approximate formula in e is released. Such long-term harmonic effects are

$$\left\langle \frac{d\Delta t_{\text{ecl}}}{dt} \right|^{(J_2^*)} = - \left(\frac{R_*}{a} \right)^2 \frac{3eJ_2^* (3+5 \cos 2\Psi_*) \sin \omega}{2\sqrt{1-e^2} (1-e^2 \sin^2 \omega)^2}, \tag{65}$$

¹¹ We assume $i = 90$ deg.

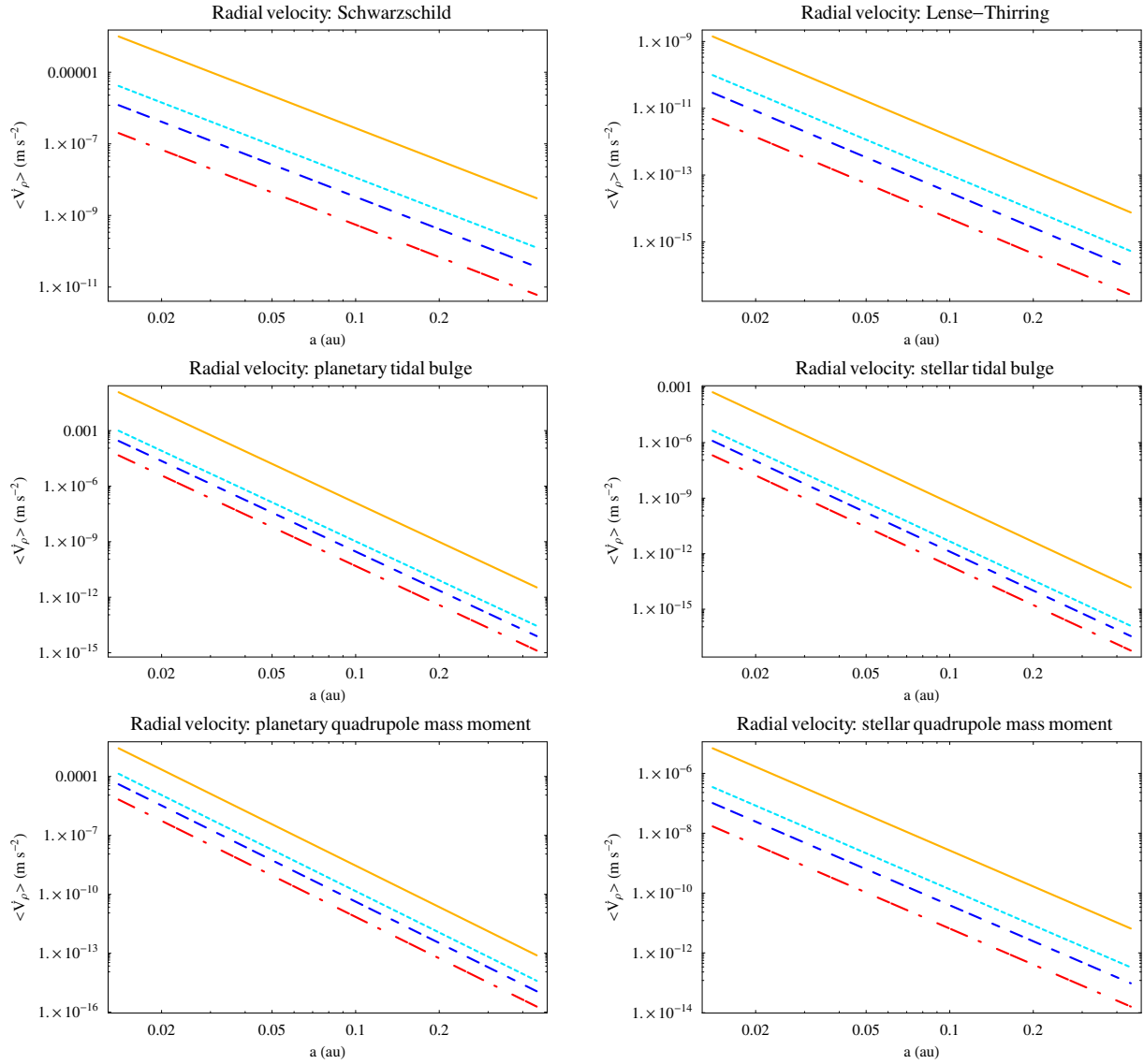


Figure 3. Maximum values of the long-term time variation $\langle \dot{V}_\rho \rangle$, in m s^{-2} , as a function of a ($0.014 \text{ au} \leq a \leq 0.449 \text{ au}$) for different values of the eccentricity: $e = 0.005$ (red dash-dotted line), $e = 0.03$ (blue dashed line), $e = 0.1$ (light blue dotted line), $e = 0.6$ (yellow continuous line). For the stellar and planetary physical parameters, and for the inclination of the orbit to the plane of the sky and to the star/planet equators we used the standard values of Table 2. We fixed the periastron at $\omega = 90$ deg.

$$\left\langle \frac{d\Delta t_{\text{ecl}}}{dt} \Big|^{(j_2^{\text{P}})} \right\rangle = - \left(\frac{r_{\text{P}}}{a} \right)^2 \frac{3e j_2^{\text{P}} (3 + 5 \cos 2\psi_{\text{P}}) \sin \omega}{2\sqrt{1-e^2} (1-e^2 \sin^2 \omega)^2}, \quad (66)$$

$$\begin{aligned} \left\langle \frac{d\Delta t_{\text{ecl}}}{dt} \Big|^{(\text{tid p})} \right\rangle &= \\ &= \left(\frac{M_\star}{m_{\text{P}}} \right) \left(\frac{r_{\text{P}}}{a} \right)^5 \\ &= \frac{15e(-128 + 1152e^2 + 6048e^4 + 4200e^6 + 441e^8) k_{2\text{P}} \sin \omega}{64(1-e^2)^{7/2} (1-e^2 \sin^2 \omega)^2}, \end{aligned} \quad (69)$$

$$\left\langle \frac{d\Delta t_{\text{ecl}}}{dt} \Big|^{(\text{GE})} \right\rangle = - \left(\frac{\mathcal{R}_q}{a} \right) \frac{12e\sqrt{1-e^2} \sin \omega}{(1-e^2 \sin^2 \omega)^2}, \quad (67)$$

$$\left\langle \frac{d\Delta t_{\text{ecl}}}{dt} \Big|^{(\text{GM})} \right\rangle = \left(\frac{GS_\star}{c^2 n a^3} \right) \frac{24e \cos \Psi_\star \sin \omega}{(1-e^2 \sin^2 \omega)^2}, \quad (68)$$

$$\begin{aligned} \left\langle \frac{d\Delta t_{\text{ecl}}}{dt} \Big|^{(\text{tid } \star)} \right\rangle &= \\ &= \left(\frac{m_{\text{p}}}{M_{\star}} \right) \left(\frac{R_{\star}}{a} \right)^5 \\ &\quad \frac{15e(-128+1152e^2+6048e^4+4200e^6+441e^8)k_{2\star} \sin \omega}{64(1-e^2)^{7/2}(1-e^2 \sin^2 \omega)^2} \end{aligned} \quad (70)$$

$$\begin{aligned} \left\langle \frac{d\Delta t_{\text{ecl}}}{dt} \Big|^{(\text{X})} \right\rangle &= \left(\frac{K_{\text{X}}}{n^2} \right) \frac{3e}{(1-e^2)^{3/2}(1-e^2 \sin^2 \omega)^3} \\ &\quad \left[\sum_{k=1}^6 (l_i l_j)_k \mathfrak{S}_k(\Omega, \omega, \Psi_{\star}) \right] + \\ &\quad + \mathcal{O}(e^2), \end{aligned} \quad (71)$$

where $(l_i l_j)_k$, $k = 1 \dots 6$ are to be intended as the six products $l_x^2, l_x l_y, l_x l_z, l_y^2, l_y l_z, l_z^2$ of the components of \hat{l}_{X} , while each of the six \mathfrak{S}_k , $k = 1 \dots 6$ is a linear combination of trigonometric functions whose arguments are, in turn, linear combinations of $\Omega, \omega, \Psi_{\star}$. Note that eq. (65)-eq. (71) vanish in the limit $e \rightarrow 0$, as expected, while they do not vanish for $\Psi_{\star} = 0$.

It is interesting to note that the same considerations of Section 4.3 concerning the relative strengths of the tidally-induced effects on the radial velocity hold also in this case. Indeed, according to eq. (69)-eq. (70) the ratio of the planet-to-star tidal effects is equal just to eq. (58).

5.2 Numerical evaluations

For the typical star-planet scenario of Table 2 we have

$$\begin{aligned} \left\langle \frac{d\Delta t_{\text{ecl}}}{dt} \Big|^{(\text{tid p})} \right\rangle &\leq 3 \times 10^{-7}, \\ \left\langle \frac{d\Delta t_{\text{ecl}}}{dt} \Big|^{(\text{GE})} \right\rangle &\leq 2 \times 10^{-7}, \\ \left\langle \frac{d\Delta t_{\text{ecl}}}{dt} \Big|^{(j_2^{\text{p}})} \right\rangle &\leq 3 \times 10^{-8}, \\ \left\langle \frac{d\Delta t_{\text{ecl}}}{dt} \Big|^{(j_2^{\star})} \right\rangle &\leq 2 \times 10^{-9}, \\ \left\langle \frac{d\Delta t_{\text{ecl}}}{dt} \Big|^{(\text{tid } \star)} \right\rangle &\leq 1 \times 10^{-9}, \\ \left\langle \frac{d\Delta t_{\text{ecl}}}{dt} \Big|^{(\text{GM})} \right\rangle &\leq 4 \times 10^{-11}, \end{aligned} \quad (72)$$

The effect of a distant perturbing body X is comparable to, or even larger than eq. (72). Indeed, for $m_{\text{X}} = m_{\text{Jup}}, r_{\text{X}} = 0.1 - 1$ au and $l_z = 0$, i.e by assuming coplanarity with the perturbed planet, we have

$$\left\langle \frac{d\Delta t_{\text{ecl}}}{dt} \Big|^{(\text{Jup})} \right\rangle \lesssim 1 \times 10^{-5} - 1 \times 10^{-8}. \quad (73)$$

If we assume an Earth-sized perturbing body X at $0.1 - 1$ au we have

$$\left\langle \frac{d\Delta t_{\text{ecl}}}{dt} \Big|^{(\text{Ear})} \right\rangle \lesssim 4 \times 10^{-8} - 4 \times 10^{-11}. \quad (74)$$

Figure 4 illustrates the magnitude of the upper bound of $\langle \Delta t_{\text{ecl}} \rangle$ for all the dynamical effects considered, with the exception of X, as a function of the semi-major axis for different values of the eccentricity.

5.3 The measurability accuracy

Concerning the measurability of Δt_{ecl} , Jordán & Bakos (2008) point out that it would be dominated by the uncertainties in the time of the secondary eclipse $t_{2\text{ecl}}$ which is evaluated by them to be of the order of about $\sigma_{t_{2\text{ecl}}} \approx 80$ s. Thus, it is reasonable to put

$$\sigma_{\Delta t_{\text{ecl}}} \approx \frac{\sigma_{t_{2\text{ecl}}}}{\mathfrak{N}_{2\text{tr}}^{3/2}}, \quad (75)$$

where $\mathfrak{N}_{2\text{tr}}$ is the number of secondary transits observed. By posing $\tau = 10$ yr and assuming $\mathfrak{N}_{2\text{tr}} = 10^3$ it is possible to obtain

$$\sigma_{\Delta t_{\text{ecl}}} \approx 8 \times 10^{-12}. \quad (76)$$

Thus, all the effects of eq. (72) would be measurable.

6 THE VARIATION OF THE TRANSIT PERIOD IN ELLIPTIC ORBITS

Another important directly measurable quantity in transiting exoplanets is the temporal interval P_{tr} between successive primary transits (Miralda-Escudé 2002; Agol et al. 2005; Nesvorný & Morbidelli 2008; Nesvorný 2009; Veras & Ford 2009; Payne et al. 2010). To compute the variation of the transit period P_{tr} in elliptic orbits we will make use of the so-called guiding center approximation (Murray & Dermott 2000). In it, the Keplerian motion of a test particle p moving along an elliptic orbit with focus F is described in a suitable rotating reference frame $\{x' y'\}$. Referring to Figure 2.8 of Murray & Dermott (2000) for the orientation of the axes, the guiding center G is the origin of such a frame. It moves with angular speed equal to the mean motion n along a circle centered in F and having radius equal to the semi-major axis a . By orienting the y' axis tangentially the guiding center's circle towards the motion of the test particle and the x' axis perpendicularly to it from F to p, it turns out (Murray & Dermott 2000)

$$\begin{aligned} x' &= r \cos(f - \mathcal{M}) - a, \\ y' &= r \sin(f - \mathcal{M}). \end{aligned} \quad (77)$$

Concerning the argument of the harmonic functions in eq. (77), the exact relation between f and \mathcal{M} can be derived from eq. (8). It is (Capderou 2005)

$$\mathcal{M} = 2 \arctan \left[\sqrt{\frac{1-e}{1+e}} \tan \left(\frac{f}{2} \right) \right] - \frac{e\sqrt{1-e^2} \sin f}{(1+e \cos f)}. \quad (78)$$

A useful approximation of eq. (78) is (Roy 2005)

$$\mathcal{M} = f - 2e \sin f + \frac{3}{4}e^2 \sin 2f + \mathcal{O}(e^3). \quad (79)$$

As far as the transit period P_{tr} is concerned, from the choice of the axes in the rotating frame it turns out that the component relevant to such a phenomenon is y' . Thus, the departure of P_{tr} from the Keplerian orbital period $P_{\text{b}} = 2\pi/n$

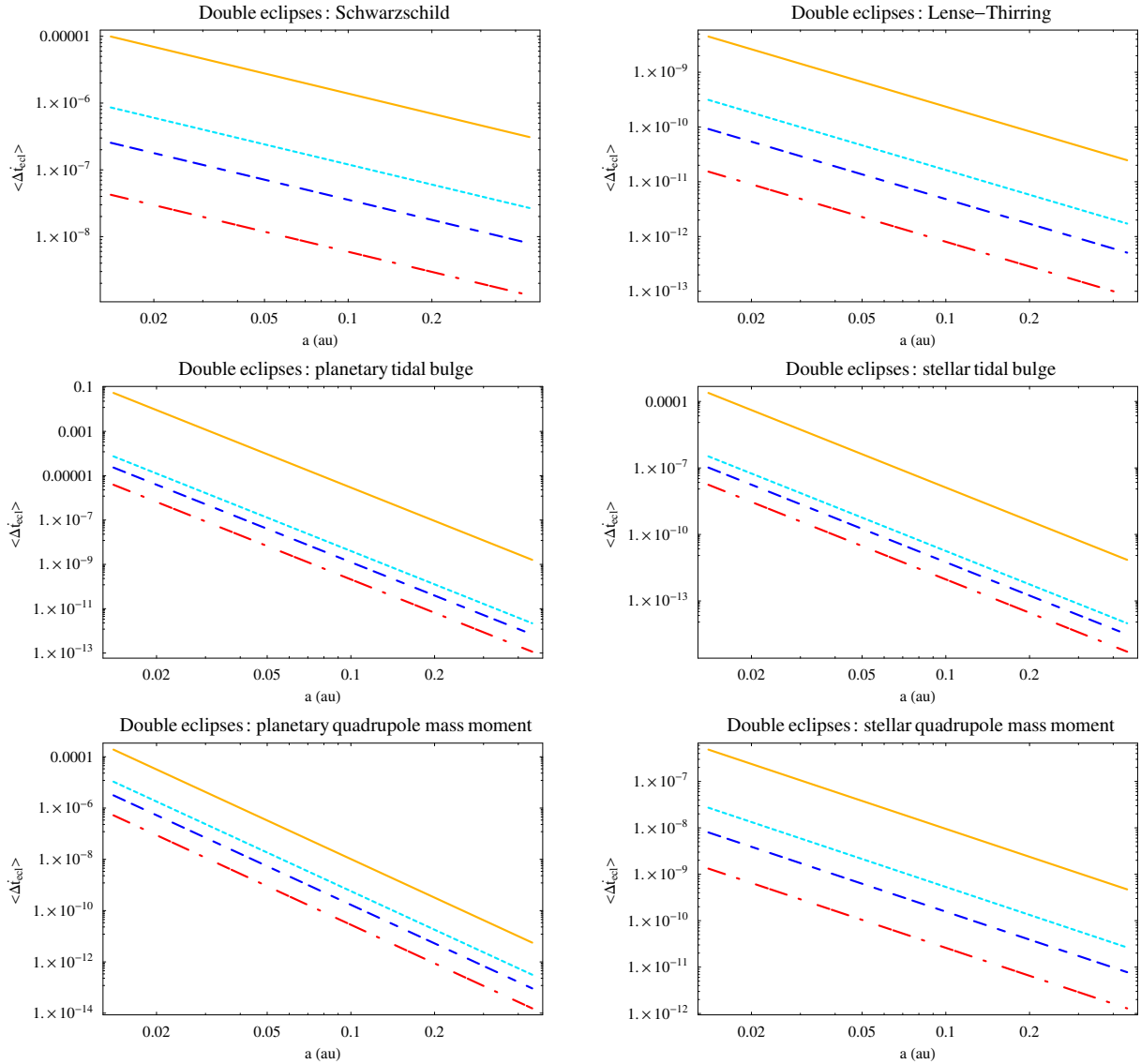


Figure 4. Maximum values of the long-term time variations $\langle \dot{\Delta} t_{\text{ecl}} \rangle$ as a function of a ($0.014 \text{ au} \leq a \leq 0.449 \text{ au}$) for different values of the eccentricity: $e = 0.005$ (red dash-dotted line), $e = 0.03$ (blue dashed line), $e = 0.1$ (light blue dotted line), $e = 0.6$ (yellow continuous line). For the stellar and planetary physical parameters, and for the inclination of the orbit to the plane of the sky and to the star/planet equators we used the standard values of Table 2. We fixed the periastron at $\omega = 90$ deg.

is due to the overall change of y' over one orbital revolution. Since the linear speed of the guiding center is $v_G = na$,

$$P_{\text{tr}} = P_b + \frac{\Delta y'}{v_G} = \frac{2\pi}{n} (1 + \lambda_{\text{tr}}), \quad (80)$$

with

$$\lambda_{\text{tr}} \doteq \frac{\Delta y'}{2\pi a}, \quad (81)$$

in which $\Delta y'$ is the variation of y' per orbit, i.e. integrated over one orbital period. By using the first term of order $\mathcal{O}(e)$

in the approximation of eq. (79) and¹²

$$y' \approx 2ae \sin f, \quad (82)$$

it is possible to explicitly compute the effects of several dynamical perturbations on P_{tr} . The averaged time variation of it can straightforwardly be computed from eq. (1) for $Y \rightarrow y'/na$, with y' conveniently given by eq. (82). A common feature of the results that we are going to show below is that non-zero long-term variations of P_{tr} occur for all the dynamical effects considered; they do not vanish in the limit $e \rightarrow 0$.

¹² As a consequence, p moves about G in the opposite sense with respect to G about F on a 2:1 ellipse of period $2\pi/n$ (Murray & Dermott 2000).

6.1 The effect of the stellar oblateness

A straightforward calculation yields the following non-zero long-term harmonic effect.

$$\begin{aligned} \left\langle \frac{dP_{\text{tr}}}{dt} \right\rangle^{(J_2^*)} &= -\frac{3J_2^*}{64(1-e^2)^3} \left(\frac{R_*}{a}\right)^2 \times \\ &\times \left[-(2+e^2)(-8+5e^2)(1+3\cos 2\Psi_*) - \right. \\ &\left. - e^2 \left(8 + \frac{77}{2}e^2\right) \sin^2 \Psi_* \cos 2\omega \right]. \end{aligned} \quad (83)$$

Note that eq. (83) vanish neither for equatorial ($\Psi_* = 0$) nor for polar ($\Psi_* = 90$ deg) orbits.

6.2 The tidal bulges

It is found that the tidal bulges cause non-vanishing long-term secular¹³ variations of P_{tr} . They are

$$\left\langle \frac{dP_{\text{tr}}}{dt} \right\rangle^{(\text{tid p})} = \left(\frac{M_*}{m_{\text{p}}}\right) \left(\frac{r_{\text{p}}}{a}\right)^5 \frac{3(-128-464e^2+320e^4+195e^6)k_{2\text{p}}}{64(1-e^2)^6}, \quad (84)$$

$$\left\langle \frac{dP_{\text{tr}}}{dt} \right\rangle^{(\text{tid }*)} = \left(\frac{m_{\text{p}}}{M_*}\right) \left(\frac{R_*}{a}\right)^5 \frac{3(-128-464e^2+320e^4+195e^6)k_{2*}}{64(1-e^2)^6}. \quad (85)$$

Note that, also in this case, the ratio of the planet-to-star tidal effects is equal just to eq. (58), as in Section 4.3 for V_{p} and Section 5.1 for Δt_{ecl} .

6.3 The effects of general relativity

The general relativistic gravitoelectric term induces the following long-term secular variation of P_{tr} .

$$\left\langle \frac{dP_{\text{tr}}}{dt} \right\rangle^{(\text{GE})} = \left(\frac{\mathcal{R}_g}{a}\right) \frac{(24+33e^2-7e^4)}{4(1-e^2)^2}. \quad (86)$$

It is interesting to note that eq. (86) is quite different from eq.(17) by Jordán & Bakos (2008) yielding an instantaneous formula proportional to e . Also the gravitomagnetic field causes a net non-vanishing harmonic effect, which is

$$\left\langle \frac{dP_{\text{tr}}}{dt} \right\rangle^{(\text{GM})} = \left(\frac{GS_*}{c^2 na^3}\right) \frac{2\left(2 - \frac{e^2}{4}\right) \cos \Psi_*}{(1-e^2)^{3/2}}. \quad (87)$$

It vanishes for polar orbits.

6.4 The third body X

As expected, in this case the calculations are much more cumbersome. To effectively perform them, the further approximation

$$(1+e\cos f)^{-k} \approx 1 - ke\cos f, \quad k = 2, 3, 4 \quad (88)$$

is adopted. We have

$$\left\langle \frac{dP_{\text{tr}}}{dt} \right\rangle^{(\text{X})} = \left(\frac{\mathcal{K}_{\text{X}}}{n^2}\right) \frac{3(1-e^2)^2 \mathfrak{Y}(\hat{L}_{\text{X}}, \Omega, \omega, \Psi_*)}{16}, \quad (89)$$

where \mathfrak{Y} is a complicated function of the angular orbital parameters of the planet and of the position of X. As in

¹³ Indeed, a and e do not undergo long-term time variations.

the previous cases, it is not worth explicitly showing it. It is found that the long-term harmonic signal of eq. (89) does not vanish for any particular orbital configurations of both the perturbed planet p and the distant perturber X. For example, if both lie in the equatorial plane of the hosting star, eq. (89) is not zero.

6.5 Numerical evaluations

The standard scenario of Table 2 yields

$$\begin{aligned} \left\langle \frac{dP_{\text{tr}}}{dt} \right\rangle^{(\text{GE})} &= 1 \times 10^{-6}, \\ \left\langle \frac{dP_{\text{tr}}}{dt} \right\rangle^{(\text{tid p})} &= 8 \times 10^{-7}, \\ \left\langle \frac{dP_{\text{tr}}}{dt} \right\rangle^{(J_2^*)} &= 1 \times 10^{-7}, \\ \left\langle \frac{dP_{\text{tr}}}{dt} \right\rangle^{(J_2^*)} &= 8 \times 10^{-9}, \\ \left\langle \frac{dP_{\text{tr}}}{dt} \right\rangle^{(\text{tid }*)} &= 4 \times 10^{-9}, \\ \left\langle \frac{dP_{\text{tr}}}{dt} \right\rangle^{(\text{GM})} &= 1 \times 10^{-10}, \end{aligned} \quad (90)$$

The effect of a Jupiter-sized third body X at $r_{\text{X}} = 0.1 - 1$ au is of the order of $10^{-5} - 10^{-8}$. An Earth-type perturber X at the same distances would yield variations of P_{tr} of about $10^{-8} - 10^{-11}$. Figure 5 depicts the magnitude of the upper bound of $\langle \dot{P}_{\text{tr}} \rangle$ for all the dynamical effects considered, with the exception of X, as a function of the semi-major axis for different values of the eccentricity.

6.6 Measurement accuracy

Concerning the accuracy with which time variations of the transit period could be detected, Miralda-Escudé (2002) yields $\sigma_{\dot{P}_{\text{tr}}} \approx 10^{-13}$ over $\tau = 10$ yr. He assumes about $\mathfrak{N}_{\text{tr}} = 1000$ primary transits and an accuracy in measuring each primary transit of $\sigma_{\text{ecl}} \approx 1$ s. A similar evaluation is given by Jordán & Bakos (2008). Note that their formula of eq.(17) yields a value for the general relativistic gravitoelectric effect which is about 6 orders of magnitude smaller than ours in eq. (90); the pessimistic conclusions by Jordán & Bakos (2008) are actually based just on such a small figure. Finally, let us note that Maciejewski et al. (2010) have recently detected transit timing variations in WASP-3b ($a = 0.03$ au, $e \approx 0$, $P_{\text{b}} = 1.8$ d) over $\tau = 2$ yr (2009-2010), but they exhibit a harmonic pattern with a periodicity of about 124 d and semi-amplitude of 1.4×10^{-3} d, with no discernable secular trends. In fact, such kind of cumulatively growing patterns, which may be caused by the tidal bulges and the general relativistic gravitoelectric field according to eq. (84)-eq. (84) and eq. (86), could not have been detected since the accuracy with which P_{tr} has been measured by Maciejewski et al. (2010) is of the order of $2.4P_{\text{b}} = 4 \times 10^5$ s. Over $\tau = 2$ yr this naively translates into a potential accuracy in detecting \dot{P}_{tr} of about 6×10^{-3} . Looking at eq. (89) for X, it results that long-period harmonic effects are, in principle, possible in view of the interplay

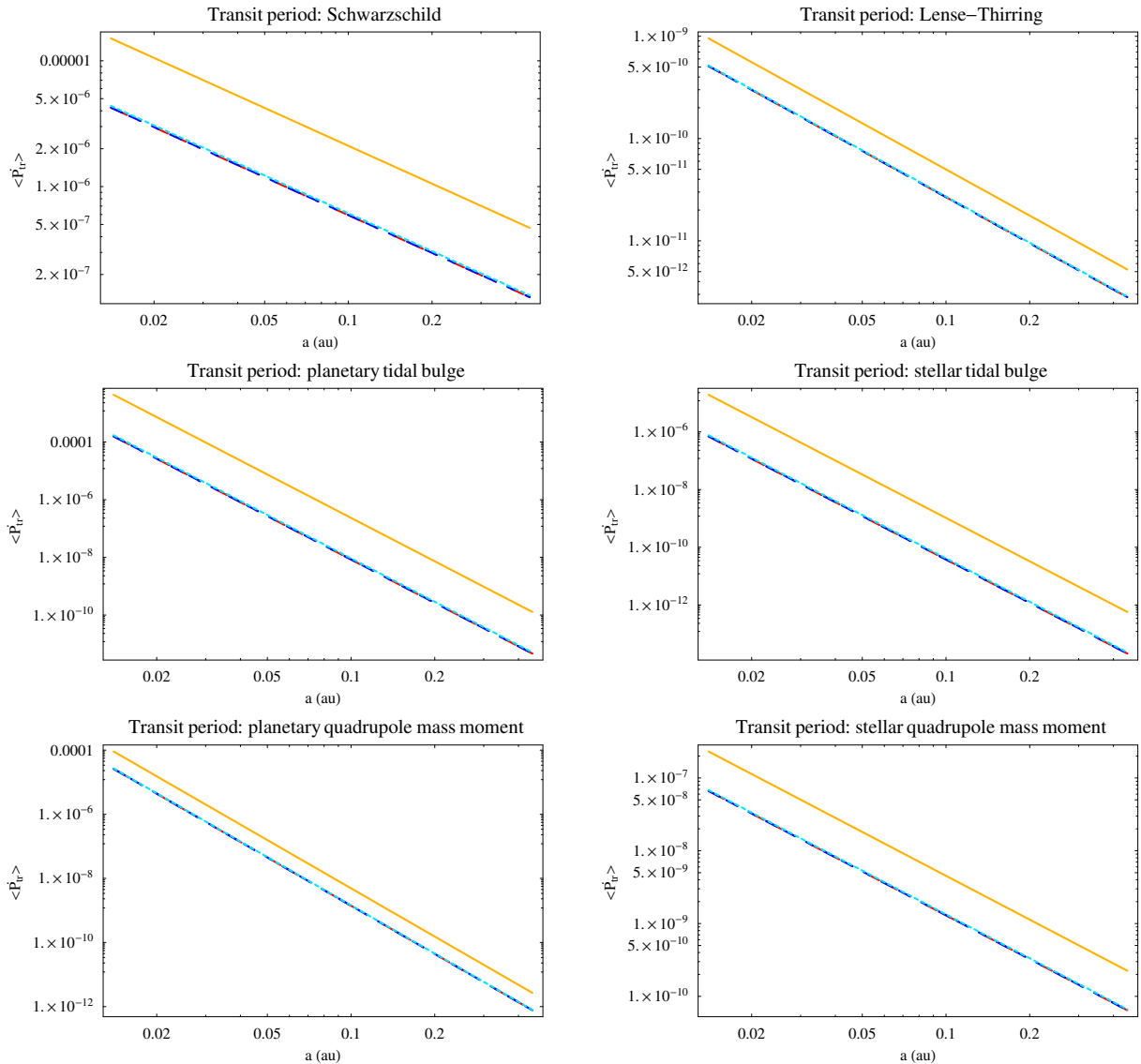


Figure 5. Maximum values of the long-term time variations $\langle \dot{P}_{\text{tr}} \rangle$ as a function of a ($0.014 \text{ au} \leq a \leq 0.449 \text{ au}$) for different values of the eccentricity: $e = 0.005$ (red dash-dotted line), $e = 0.03$ (blue dashed line), $e = 0.1$ (light blue dotted line), $e = 0.6$ (yellow continuous line). For the stellar and planetary physical parameters, and for the inclination of the orbit to the plane of the sky and to the star/planet equators we used the standard values of Table 2. We fixed the periastron at $\omega = 90 \text{ deg}$.

between the node and the periastron of WASP-3b entering \mathfrak{N} ; recall that they slowly change because of the oblateness, tidal bulges, general relativity and a X themselves. However, the figures for $\langle \dot{P}_{\text{tr}} \rangle$ in Section 6.5, valid for plausible values of \mathcal{K}_X , do not allow to obtain magnitudes as large as¹⁴ 10^{-3} d .

7 SUMMARY AND CONCLUSIONS

We looked at the impact of several classical and general relativistic dynamical perturbations on directly observable

quantities in transiting exoplanets. We considered the centrifugal oblateness of both the hosting star and the planet due to their rotations, the tidal bulges mutually raised by both the star and the planet on each other, and a distant third body X as Newtonian effects. Concerning general relativity, we took into account both the so called gravitoelectric, Schwarzschild and the gravitomagnetic, Lense-Thirring perturbations. The observables considered are the transit duration Δt_d , the radial velocity V_ρ , the time interval Δt_{ecl} elapsed between primary and secondary eclipses, and the time span P_{tr} between successive primary transits.

We analytically worked out, in an uniform and straightforward way, the long-term, i.e. averaged over one orbital revolution, temporal variations of such quantities caused by the aforementioned non-Keplerian features of motion. We did not restrict ourselves to circular orbits.

¹⁴ They can be obtained by multiplying $\langle \dot{P}_{\text{tr}} \rangle$ by P_b .

For all the dynamical effects considered we released numerical evaluations of their magnitudes by adopting a typical exoplanetary scenario involving a Jupiter-sized planet closely ($a = 0.04$ au) revolving around a main sequence Sun-like star along a moderately eccentric orbit ($e = 0.07$) lying in the orbital plane of the parent star ($\Psi_* = 0$). The rotation of the planet has been assumed synchronized with its orbital frequency because of tidal effects, and an edge-on configuration ($i = 90$ deg) has been assumed. For each observable considered, we gave an order-of-magnitude evaluation of the accuracy with which it could be measured over an observational time span $\tau = 10$ yr. In view of the wide distribution of orbital configurations which is expected to characterize the numerous planets which will be discovered by the ongoing space-based Kepler mission, we also performed graphical investigations of the dependence of the effects studied on the semi-major axes a and the eccentricities e .

No net changes $\langle \dot{\Delta}t_d \rangle$ in the duration transit occur for both the tidal bulges and the Schwarzschild perturbations. Instead, the oblateness of the bodies, a distant planet X and the Lense-Thirring effect induce long-term, harmonic variations of the transit duration which do not vanish even for circular orbits. For exactly edge-on orbits ($i = 90$ deg), $\langle \dot{\Delta}t_d \rangle = 0$ in all cases. The same occur, independently of the inclination i of the orbital plane to the line of sight, for equatorial orbits ($\Psi_* = 0$), apart from X if it is not coplanar with the perturbed body. If both the planet and its perturber X lie in the same plane coinciding with the equatorial plane of the star, then $\langle \dot{\Delta}t_d \rangle = 0$. By assuming small departures from the equatorial ($\Psi_* = 15$ deg) and edge-on ($i = 87$ deg) orbital configuration, the magnitude of the upper limits of the non-zero oblateness and gravitomagnetic effects is of the order of $10^{-8} - 10^{-12}$. A jovian perturbing body X at 0.1–1 au would cause a rate of $\approx 10^{-5} - 10^{-8}$, while for an Earth-size X at the same distances we have $\langle \dot{\Delta}t_d \rangle \approx 10^{-7} - 10^{-10}$. The expected accuracy in measuring $\langle \dot{\Delta}t_d \rangle$ over $\tau = 10$ yr is about $\sigma_{\dot{\Delta}t_d} \approx 10^{-9} - 10^{-8}$.

The radial velocity V_ρ undergoes non-vanishing long-term, harmonic variations caused by all the perturbations considered only for eccentric orbits; the resulting amplitudes are proportional to e , and vanish neither for equatorial nor edge-on orbits. The largest effects, of the order of 10^{-7} m s $^{-2}$, are due to the tidal bulge raised on the planet and the general relativistic Schwarzschild term. The centrifugal oblateness of the planet causes an acceleration of the order of 10^{-8} m s $^{-2}$, while the changes due to the centrifugal oblateness and the tidal distortion of the star are of the order of 10^{-9} m s $^{-2}$. The Lense-Thirring effect amounts to $\approx 10^{-11}$ m s $^{-2}$. The perturbation of a distant Jupiter-sized body X at 0.1–1 au is $\langle \dot{V}_\rho \rangle \approx 10^{-5} - 10^{-8}$ m s $^{-2}$, while a rocky planet with the mass of the Earth located at the same distances would cause $\langle \dot{V}_\rho \rangle \approx 10^{-8} - 10^{-11}$ m s $^{-2}$. The accuracy with which it is possible to measure secular trends in the radial velocity is $\sigma_{\dot{V}_\rho} \approx 10^{-9}$ m s $^{-2}$ over $\tau = 10$ yr.

Concerning the time interval Δt_{ecl} between primary and secondary eclipses, it experiences long-term, harmonic variations only for eccentric orbits. Its amplitudes are proportional to e , and are non-vanishing for all the perturbations considered. Also in this case, the largest effects, of the order

of 10^{-7} , are due to the tidal bulge raised on the planet and the general relativistic gravitoelectric field. The centrifugal oblateness of the planet causes an effect of the order of 10^{-8} , while the variations induced by the centrifugal oblateness and the tidal distortion of the star are of the order of 10^{-9} . The effect due to the general relativistic gravitomagnetic field is as large as about 10^{-11} . The perturbation of a jovian-type body X at 0.1–1 au is $\langle \dot{\Delta}t_{\text{ecl}} \rangle \approx 10^{-5} - 10^{-8}$, while a terrestrial planet at the same distances would induce $\langle \dot{\Delta}t_{\text{ecl}} \rangle \approx 10^{-8} - 10^{-11}$. The expected accuracy in measuring $\langle \dot{\Delta}t_{\text{ecl}} \rangle$ over $\tau = 10$ yr is about $\sigma_{\dot{\Delta}t_{\text{ecl}}} \approx 10^{-12}$.

All the dynamical effects considered causes long-term variations of the transit period P_{tr} . They do not vanish for circular orbits. While the signals due to the stellar and planetary oblateness, the gravitomagnetic field and a third body X are harmonic, those induced by the tidal bulges and the gravitoelectric field are secular rates. The largest effect, of the order of 10^{-6} , is the trend due to general relativity (Schwarzschild). The rate due to the planetary tidal bulge is 8×10^{-7} , while that due to the star's tidal distortion is 2 orders of magnitude smaller. The amplitudes of the signals caused by the planetary and the stellar oblateness are 1×10^{-7} and 8×10^{-9} , respectively. The gravitomagnetic effect has an amplitude of the order of 10^{-10} . The action of a distant Jupiter-like planet X at 0.1–1 au is $\langle \dot{P}_{\text{tr}} \rangle \approx 10^{-5} - 10^{-8}$, while an Earth-type planet at the same distances would cause $\langle \dot{P}_{\text{tr}} \rangle \approx 10^{-8} - 10^{-11}$. It should be possible to measure long-term changes in P_{tr} with an accuracy of about 10^{-13} over $\tau = 10$ yr.

Our results may be useful in focussing the research on some specific exoplanets or classes of exoplanets, particularly tailored to measure a given dynamical effect of interest. Moreover, they should allow to better evaluate the systematic uncertainty in the determination of a given stellar/planetary physical parameter induced by the other perturbations which are to be considered as sources of bias. Moreover, our approach can, in principle, be extended also to other scenarios and dynamical features of motion involving, e.g., natural and artificial bodies in our solar system in order to suitably design new tests of general relativity and modified models of gravity. The latter issues, along with a more detailed quantitative analysis of different, specific exoplanetary scenarios, may be the subject of further researches.

ACKNOWLEDGMENTS

I gratefully thank the referee for valuable suggestions and remarks.

REFERENCES

- Adams F.C., Laughlin G., 2006a, ApJ, 649, 992
- Adams F.C., Laughlin G., 2006b, ApJ, 649, 1004
- Adams F.C., Laughlin G., 2006c, Int. J. Mod. Phys. D., 15, 2133

- Agol E., Steffen J., Sari R., Clarkson W., 2005, MNRAS, 359, 567
- Anderson D.R., Gillon M., Hellier C., Maxted P.F.L., Pepe F., Queloz D., Wilson D.M., Collier Cameron A., Smalley B., Lister T.A., Bentley S.J., Blecha A., Christian D.J., Enoch B., Hebb L., Horne K., Irwin J., Joshi Y.C., Kane S.R., Marmier M., Mayor M., Parley N.R., Pollacco D.L., Pont F., Ryans R., Sgransan D., Skillen I., Street R.A., Udry S., West R.G., Wheatley P.J., 2008, MNRAS, 387, L4
- Anderson D.R., Hellier C., Gillon M., TriAUD A.H.M.J., Smalley B., Hebb L., Collier Cameron A., Maxted P.F.L., Queloz D., West R.G., Bentley S.J., Enoch B., Horne K., Lister T.A., Mayor M., Parley N.R., Pepe F., Pollacco D., Ségransan D., Udry S., Wilson D.M., 2010, ApJ, 709, 159
- Batten A.H., 2001, Spectroscopic Binary Stars, in: Murdin P. (ed). Encyclopedia of Astronomy and Astrophysics (Bristol: Institute of Physics) p. 2992
- Borucki W.J., Koch D.; Basri G.; Batalha N.; Brown T.; Caldwell D.; Caldwell J.; Christensen-Dalsgaard J.; Cochran W.D., DeVore E.; Dunham E.W., Dupree A.K., Gautier T.N., Geary J.C., Gilliland R., Gould A., Howell S.B., Jenkins J.M., Kondo Y.; Latham D.W., Marcy G.W., Meibom S., Kjeldsen H., Lissauer J.J., Monet D.G., Morrison D., Sasselov D., Tarter J., Boss A., Brownlee D., Owen T., Buzasi D., Charbonneau D., Doyle L., Fortney J., Ford E.B., Holman M.J., Seager S., Steffen J.H., Welsh W.F., Rowe J., Anderson H., Buchhave L., Ciardi D., Walkowicz L., Sherry W., Horch E., Isaacson Howard; Everett Mark E., Fischer D., Torres G., Johnson J.A., Endl M., MacQueen P., Bryson S.T., Dotson J., Haas M., Kolodziejczak J., Van Cleve J., Chandrasekaran H., Twicken J.D., Quintana E.V., Clarke B.D., Allen C., Li J., Wu H., Tenenbaum P., Verner E., Bruhweiler F., Barnes J., Prsa A., 2010, Science, 327, 977
- Capderou M., 2005, Satellites. Orbits and missions. (Paris: Springer-Verlag) p. 16
- Claret A., 1995, Astronomy and Astrophysics Supplement, 114, 549
- Collier Cameron A., Bouchy F., Hébrard G., Maxted P., Pollacco D., Pont F., Skillen I., Smalley B., Street R.A., West R.G., Wilson D.M., Aigrain S., Christian D.J., Clarkson W. I., Enoch B., Evans A., Fitzsimmons A., Fleenor M., Gillon M., Haswell C.A., Hebb L., Hellier C., Hodgkin S.T., Horne K., Irwin J., Kane S.R., Keenan F.P., Loeillet B., Lister T.A., Mayor M., Moutou C., Norton A.J., Osborne J., Parley N., Queloz D., Ryans R., TriAUD A.H.M.J., Udry S., Wheatley P.J., 2007, MNRAS, 375, 951
- Collier Cameron A., Guenther E., Smalley B., McDonald I., Hebb L., Andersen J., Augusteijn Th., Barros S.C.C., Brown D.J.A., Cochran W.D., Endl M., Fossey S.J., Hartmann M., Maxted P.F., Pollacco D., Skillen I., Telting J., Waldmann I.P., West R.G., 2010, MNRAS, 407, 507
- Cowling T.G., 1938, MNRAS, 98, 734
- Cunningham L.E., 1970, Celest. Mech. Dyn. Astron., 2, 207
- Deeg H.-J., 1998, Photometric Detection of Extrasolar Planets by the Transit-Method. In: Rebolo R., Martín E.L., Zapatero Osorio M.R., Brown dwarfs and extrasolar planets, Proceedings of a Workshop held in Puerto de la Cruz, Tenerife, Spain, 17-21 March 1997, ASP Conference Series vol. 134, pp. 216-223
- Ford E.B., Quinn S.N., Veras D., 2008, ApJ, 678, 1407
- Gellert W., Gottwald S., Hellwich M., Kästner H., Künstner H. (eds.), 1989, Spherical Trigonometry. §12 in VNR Concise Encyclopedia of Mathematics, 2nd ed. (New York: Van Nostrand Reinhold), pp. 261-282
- Gillon M., Smalley B., Hebb L., Anderson D.R., TriAUD A.H.M.J., Hellier C., Maxted P.F.L., Queloz D., Wilson D.M., 2009, A&A, 496, 259
- Gould A., Chanamé J., 2004, ApJS, 150, 455
- Heyl J.S., Gladman B.J., 2007, MNRAS, 377, 1511
- Hogg D., Quinlan G., Tremaine S., 1991, AJ, 101, 2274
- Howard A.W., Johnson J.A., Marcy G.W., Fischer D.A., Wright J.T., Bernat D., Henry G.W., Peek K.M.G., Isaacson H., Aps K., Endl M., Cochran W.D., Valenti J. A., Anderson J., Piskunov N.E., 2010, ApJ, 721, 1467
- Iorio L., 2006, New Astronomy, 11, 490
- Iorio L., 2007, ApSS, 312, 331
- Iorio L., 2010, ApSS, doi:10.1007/s10509-010-0468-x
- Jordán A., Bakos G.Á., 2008, ApJ, 685, 543
- Lense J., Thirring H., 1918, Phys. Z., 19, 156
- Li L.-S., 2010, ApSS, 327, 59
- Maciejewski G., Dimitrov D., Neuhäuser R., Niedzielski A., Raetz St., Ginski Ch., Adam Ch., Marka C., Moualla M., Mugrauer M., 2010, MNRAS, 407, 2625
- Mashhoon B., Gravitoelectromagnetism: A Brief Review, 2007, in: Iorio L. (ed.) The Measurement of Gravito-magnetism: A Challenging Enterprise, (Hauppauge: Nova Publishers), pp. 29-39
- Miralda-Escudé J. 2002, ApJ, 564, 1019
- Montenbruck O., Gill E., 2000, Satellite Orbits. (Berlin: Springer Verlag)
- Murray C.D., Dermott S.F., 2000, Solar System Dynamics (New York: Cambridge Univ. Press)
- Narita N., Sato B., Hirano T., Tamura M., 2009, PASJ, 60, L35
- Nesvorný D., Morbidelli A., 2008, ApJ, 688, 636
- Nesvorný D., 2009, ApJ, 701, 1116
- Pál A., Kocsis B., 2008, MNRAS, 389, 191
- Payne M.J., Ford E.B., Veras D., 2010, ApJ, 712, L86
- Pijpers F.P., 1998, MNRAS, 297, L76
- Pijpers F.P., 2003, A&A, 402, 683
- Pireaux S., Standish E.M., Pitjeva E.V., Rozelot J.-P., 2007, Solar quadrupole moment from planetary ephemerides: present state of the art, in: Proceedings of the International Astronomical Union (2006), 2, 473. (Cambridge: Cambridge Univ. Press)
- Queloz D., Anderson D., Collier Cameron A., Gillon M., Hebb L., Hellier C., Maxted P., Pepe F., Pollacco D., Ségransan D., Smalley B., Udry S., West R., 2010, A&A, 517, L1
- Ragozzine D., Wolf A.S., 2009, ApJ, 698, 1778
- Roy A.E., 2005, Orbital Motion. Fourth Edition. (Bristol: Institute of Physics)
- Soffel M.H., 1989, Relativity in Astrometry, Celestial Mechanics and Geodesy. (Berlin: Springer Verlag)
- Sterne T.E., 1940, Proceedings of the National Academy of Sciences of the United States of America, 26, 36
- Tingley B., Sackett P.D., 2005, ApJ, 627, 1011
- Torres G., Winn J.N., Holman M.J., 2008, ApJ, 677, 1324
- Veras D., Ford E.B., 2009, Identifying Non-transiting Terrestrial Planets with Transit Timing Data, in Transiting Planets, Proceedings of the International Astronomical

- Union, IAU Symposium, Volume 253, Cambridge University Press, Cambridge, p. 486
- Vrbik J., 2005, *Celest. Mech. Dyn. Astron.*, 91, 217
- West R.G., Anderson D.R., Gillon M., Hebb L., Hellier C., Maxted P.F.L., Queloz D., Smalley B., Triaud A.H.M.J., Wilson D.M., Bentley S.J., Collier Cameron A., Enoch B., Horne K., Irwin J., Lister T.A., Mayor M., Parley N., Pepe F., Pollacco D., Segransan D., Spano M., Udry S., Wheatley P.J., *AJ*, 137, 4834
- Winn J.N., Johnson J.A., Albrecht S., Howard A.W., Marcy G.W., Crossfield I.J., Holman M.J., 2009, *ApJ*, 703, L99
- Zwillinger D. (ed.), 1995, *Spherical Geometry and Trigonometry*. §6.4 in *CRC Standard Mathematical Tables and Formulae*. (Boca Raton, FL: CRC Press), pp. 468-471